



5-2001

Real-time system for determining corn plant population in-situ at harvest time

Newman Edward Webb II

Follow this and additional works at: https://trace.tennessee.edu/utk_gradthes

Recommended Citation

Webb, Newman Edward II, "Real-time system for determining corn plant population in-situ at harvest time." Master's Thesis, University of Tennessee, 2001.
https://trace.tennessee.edu/utk_gradthes/6597

This Thesis is brought to you for free and open access by the Graduate School at TRACE: Tennessee Research and Creative Exchange. It has been accepted for inclusion in Masters Theses by an authorized administrator of TRACE: Tennessee Research and Creative Exchange. For more information, please contact trace@utk.edu.

To the Graduate Council:

I am submitting herewith a thesis written by Newman Edward Webb II entitled "Real-time system for determining corn plant population in-situ at harvest time." I have examined the final electronic copy of this thesis for form and content and recommend that it be accepted in partial fulfillment of the requirements for the degree of Master of Science, with a major in Biosystems Engineering.

William E. Hart, Major Professor

We have read this thesis and recommend its acceptance:

John B. Wilkerson, Bobby L. Bledsoe

Accepted for the Council:


Carolyn R. Hodges

Vice Provost and Dean of the Graduate School

(Original signatures are on file with official student records.)

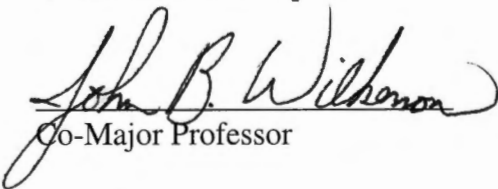
To the Graduate Council:

I am submitting a thesis written by Newman Edward Webb II entitled "Real-Time System for Determining Corn Plant Population In-Situ at Harvest Time." I have examined the final copy of thesis for form and content and recommended that it be accepted in partial fulfillment of the requirements for the degree of Master of Science, with a major in Biosystems Engineering.



William E. Hart, Major Professor

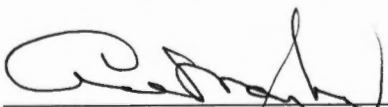
We have read this thesis and recommend its acceptance:



Co-Major Professor



Accepted for the Council:



Associate Vice Chancellor and
Dean of the Graduate School

**Real-Time System for Determining
Corn Plant Population
In-Situ at Harvest Time**

A Thesis
Presented for the
Master of Science
Degree
The University of Tennessee, Knoxville

Newman Edward Webb II
May 2001

AG-VET-MED.

Thesis

2001

.W32

Acknowledgements

I thank Dr. John B. Wilkerson, for his guidance, support, and patience with me throughout this project. I also thank Dr. William E. Hart for his constant help, friendship, and unwavering confidence in me during my time here. I also thank Dr. Bobby L. Bledsoe for his superior engineering skill and guidance throughout my career at the University. I extend a special thanks to Henry Moody whose hard work and driven nature made this project a reality. I am grateful for the excellent work and assistance of The Agricultural Engineering Shop. Paul Elliott, Craig Wagoner, and Walker Garner each contributed greatly to the fabrication of equipment used in this project.

I thank fellow graduate students Eric Simmons for his help in field-testing, and Chris Whitten for advice and heated discussions on laboratory testing. Field-testing was successful and enjoyable because of the contributions from Milan Experiment Station staff Mark Barnes, Don Gibson, Darol Copley, Jason Williams, and Dr. Blake Brown. I thank other University faculty, staff, and students: Seth Rye, Dr. Raj Raman, Dr. Ron Yoder, Jerry Peck.

Most importantly, I thank my family for their tremendous support, role modeling, and confidence in me throughout my education.

Abstract

Producers and seed companies have recently expressed interest in documenting spatial variation in corn plant population. In order to measure plant population at harvest-time, the number of corn stalks feeding into the harvester must be known. A system has been developed to measure plant population on a combine corn header. It uses a non-intrusive capacitive technique to sense corn stalks as they enter the header. Stalks pass the sensor face, and an increase in voltage is produced due to a change in sensor capacitance. This voltage increase is recorded as one corn stalk.

The system was prototyped and tested in both laboratory and field environments. Test results show that the system is capable of measuring plant population to some degree of accuracy. Accuracy measurements were based on manual stalk counts performed before harvesting. Field tests were inconclusive due to insect damage coupled with late season harvest resulted in a severely lodge crop. Accuracy was moderately correlated with speed ($r = 0.43$; $\alpha=0.05$).

Refinements in sensor head design and measurement circuitry are needed to improve measurement accuracy. Future tests should include corn stalks of various moisture contents to determine if moisture related problems exist.

Table of Contents

Chapter	Page
1. Introduction	1
Justification for Research.....	1
Objectives.....	3
2. Review of Literature.....	5
Background.....	5
Why Corn Population is Important	5
Mechanical Method.....	7
Capacitive Method	9
Theory Behind Capacitance	11
Capacitance Sensors.....	14
3. Sensor Design & Evaluation	23
Design Background	23
Impact Sensor Design.....	23
Laboratory Test Equipment.....	24
Laboratory Testing	26
Field Test.....	27
Capacitance Based Sensor Design.....	28
Design Overview.....	28
Sensor Head and Mounting Bracket Design	30
Signal Processing Hardware	32
Frequency Generation	37
Power Supply	37
Data Acquisition System	40
Data Post-Processing	40
Laboratory and Field Testing.....	45
Field Test Equipment	45
Laboratory Test	46
Water Standard.....	46
Comparison Test	48
Field Test.....	49
4. Results.....	51
Laboratory Evaluation.....	51
Water Standard	51
Comparison Test.....	52
Field Evaluation.....	55
Tractor-Mounted Sensor Test	56

Chapter	Page
Preliminary Combine-Mounted Sensor Test	56
Dynamic Limitations	57
5. Conclusions and Recommendations	59
Conclusions	59
Recommendations	59
System refinements	59
Additional Testing	61
Reference.....	62
Appendices	65
Appendix A	66
Appendix B	70
Appendix C	83
Appendix D	86
Vita.....	90

List of Figures

Figure		Page
1.	Combine harvesting point rows due to irregularly shaped field	8
2.	Mounting location of capacitance sensor.....	10
3.	Dielectric material separating 2 parallel plates	12
4.	Field lines of single plate capacitor	15
5.	Capacitance field lines being focused with guard ring.....	16
6.	Capacitance fringe field lines as a function of distance	17
7.	Single-ended capacitance measurement methods.....	19
8.	Capacitance bridge measurement circuit	21
9.	Pictorial representations of impact sensors	25
10.	Test stand used to evaluate sensor designs under controlled conditions.....	26
11.	Block diagram of system components.....	29
12.	Assembly drawing of sensor head and bracket assembly	31
13.	Mounting location of capacitance sensor	33
14.	Signal processing circuit schematic	36
15.	Frequency generation circuit schematic	38
16.	Power supply circuit schematic	39
17.	Flow chart of micrologger program.....	41
18.	Flow chart of MATLAB® program	42
19.	Graphs illustrating data processing steps of 8 stalks at 0.4 mph	44

Figure	Page
20. Tractor-mounting bracket used to accurately position sensor face a defined distance from the stalks at an operating height.....	47
21. Test grid measurement locations and sensor field lines	47
22. Mounting arrangement of prototype and commercial sensor on test stand	48
23. Prototype sensor's sensitivity resulting from electric field strength in the presence of water	52
24. Distribution of errors from the October, 2000 laboratory test.....	54
25. Distribution of errors from the October, 2000 tractor-mounted sensor test	57
26. Circuit schematic of processing circuit to replace software	60

Chapter 1--Introduction

Justification for Research

Over the last decade or so precision farming has been reluctantly embraced by producers as a way to increase yields and profits. Producers saw precision farming as “something just for a small brotherhood of cornfield tinkers-techies and early innovators” that have nothing else better to do with their time (Hillyer and Miller, 2000). However, this is not the case today where manufacturers are pushing precision farming as the future of agriculture. Presently 13% of U.S. farms have this capability and this percentage is on the rise (Hillyer and Miller, 2000). For this reason manufacturers are examining ways to increase the accuracy of yield maps so both manufacturers and producers benefit from the use of this technology.

One reason for poor yields is plant population. Detailed plant population maps can be produced from geo-referenced plant population data. When used in conjunction with yield maps, comparisons can be made. Causes of low germination rates can then be examined and a solution implemented. For example, one possible solution could be to adjust planting rates the following year in these areas depending on what the situation warrants (Harrington, 2000).

Yield maps give the producer valuable information on crop development by providing a way of visually identifying spatial variability in combined crops (Stafford, et al., 1997). Yield maps are generated from data collected from sensors on-board the harvester that have spatial coordinates associated with them. Yield data is based on the

harvester's theoretical swath width all the time; when in fact this is not always the case. The effective swath width is a true representation of the harvester's actual swath width and changes due to point rows and operator error. This is a significant source of error since all commercial systems assume a constant swath width (Stafford, et al., 1997).

Several different methods can be considered for measuring plant population. These include optical sensors, capacitance proximity sensors, piezo-electric impact sensors, and ultra-sonic sensors. Optical sensors generally have an emitter that produces a light-beam and a detector that receives it. Moody (1998) used this concept to develop a cotton yield monitor. When the beam illuminates an object, its presence is recorded. However, optical sensors do not have the ability to distinguish between materials within their range, and accuracy is reduced in dusty environments.

Capacitance proximity sensors use a material's dielectric property to electrically measure the material, and are used in liquid level sensing, touch sensing, and keyswitches. Capacitance sensors have the ability to distinguish between materials located within its sensing range due to the fact that all materials have different dielectric constants. These sensors are sometimes affected by extremes of humidity that saturate the sensed objects with water; thus, eliminating the ability of the sensor to distinguish between objects (Baxter, 1997).

Piezo-electric sensors are used in almost every conceivable application requiring measurement of dynamic changes such as pressure, force, and acceleration. The sensor consists of a die-cut piezo polymer substrate, in a thin film, that rubs against itself in the presence of a force. The faster the two materials rub, the higher the voltage output (MSI,

1998). The draw back to piezo-electric sensors is that dynamic movement of the piezo polymer must occur before any output is produced. This leads to problems protecting the delicate piezo-film in harsh environments since it is an intrusive sensor.

Ultra-sonic sensors generally use an emitter that produces a sound and a detector that receives it. They are used most often for proximity detection, and in certain situations are used to detect differences in material properties. The emitter produces a sound and an object absorbs the sound waves keeping them from being detected. Detection of different materials is accomplished by determining how much sound the detector receives after absorption from an object. Ultra-sonic sensors are affected by rain, dust, fog, and noise filled environments, which cause sensor error (Warring and Gibilisco, 1985).

Attempts have been made to measure swath width on a combine corn head and the results have been mixed. Researchers at the University of Missouri developed a sensor based on a mechanical approach. However, problems with weeds caused over-counting at slow ground speeds (Birrell and Sudduth, 1995).

Stephen W. Nichols (2000) holds a patent for a method and apparatus for counting crops. More specifically, he proposed a nonintrusive sensing method that can be mounted on a combine for counting corn population. However, literature contains no documented testing information for his technique.

Objectives

The overall objective of this project is to develop a method to accurately count corn stalk population at the combine corn header over a wide range of stalk moisture

contents. To obtain this goal, the following sub-objectives were identified: (1) design and construct a prototype sensor and circuit to count corn stalk population, (2) develop data acquisition and processing systems to evaluate the sensing unit, and (3) test the sensor system in both laboratory and field conditions.

Chapter 2--Review of Literature

Background

Producers and seed companies have recently expressed interest in documenting spatial variation in corn plant population at harvest-time. Plant population is one of the most important yield-determining factors, and the ability to plant variable-rates of seed has been present for some time (Harrington, 2000). However, generation of variable-rate seed prescriptions is very difficult, without site-specific knowledge of past plant population.

Why Corn Population Is Important

Corn yield variability depends on numerous factors: plant population, soil moisture, soil compaction, weed pressure, fertility, pH, disease, and insects. However, research has shown that plant population is the predominate factor affecting yield (Harrington, 2000). The University of Tennessee recommendations suggest optimum populations up to 28,000 plants per acre (Norman, 2000). However, 18,000 plants per acre may be more profitable on land with yield potential less than 100 bu/ac (Harrington, 2000). Barbossa's (1996) research indicates that yield potential is highly variable within a field. In fact he estimated yield potentials to vary between 70 and 140 bu/ac in a 22.5-acre field in West Tennessee. It follows that the ability to plant seed variable-rate will increase profitability by reducing the seeding rate where high populations are not justified by yield potential. However, seeding rate is not the only factor that affects final plant population.

Germination rates and plant mortality also play a major role in stand loss. Because of the complexities of the system, “ an actual assessment of spatial plant population patterns in farm fields is the first step in developing meaningful strategies for varying corn seeding rates” (Doerge, 1999).

A combine-mounted sensing system capable of measuring corn population during the harvest operation could provide another substantial benefit. Assuming corn population sensors are mounted on each row of the corn head, they will also be able to determine which rows are being fed into the combine. Thus, this enables real-time swath width measurement. Swath width measurement would be a significant improvement for grain yield monitors. To better understand the importance of swath-width, consider how grain yield monitors measure yield in bushels per acre. Instantaneous yield is calculated by the following equation.

$$Y = K \frac{Q_{\text{grain}}}{S \rho_{\text{grain}} V} \quad \text{Equation I}$$

where S = swath width being harvested by the combine (ft)

Q_{grain} = grain flow rate into the combine (lb/s)

K = unit conversion constant ($29,700 \frac{s \cdot mi \cdot ft}{hr \cdot ac}$)

Y = yield (bu/ac)

ρ = grain density (lb/bu)

V = combine ground speed (mph)

Grain mass flow rate (Q_{grain}) is measured at harvest. Grain density (ρ) is dependent on grain type and moisture content. Variations in grain density is typically automatically compensated for by use of an in-line moisture sensor. Ground speed (V) is measured from the combine power-train transmission, radar, or GPS. The swath width (S) is adjusted manually on all commercial systems. However, most producers set the width and never change it regardless of the true effective swath width.

Swath width variation is one of the most significant errors present in grain yield monitors today (Han, et al., 1997). Combine swath width is determined by the total number of feeding rows possible or the grain platform width. For example, a six-row corn header is assumed to have six rows feeding all the time. However, point rows can occur throughout a field and missing plants (skips) are always possibilities. Figure 1 illustrates how irregularly shaped fields cause the header to be at an angle with the edge of the field, leading to point row error. When these conditions occur yield monitors show less yield than is actually present. Because of this ever-present error, measuring swath width in real-time is essential to accurate yield determination (Reitz, 1996).

Mechanical Method

Birrell and Sudduth (1995) developed an intrusive sensor to measure the number of stalks feeding into the combine corn header. The sensor consisted of a spring-loaded rod attached to a rotary potentiometer, mounted in front of the gathering chains of the combine row dividers. The rod was aligned perpendicular to the corn row, so that as the combine

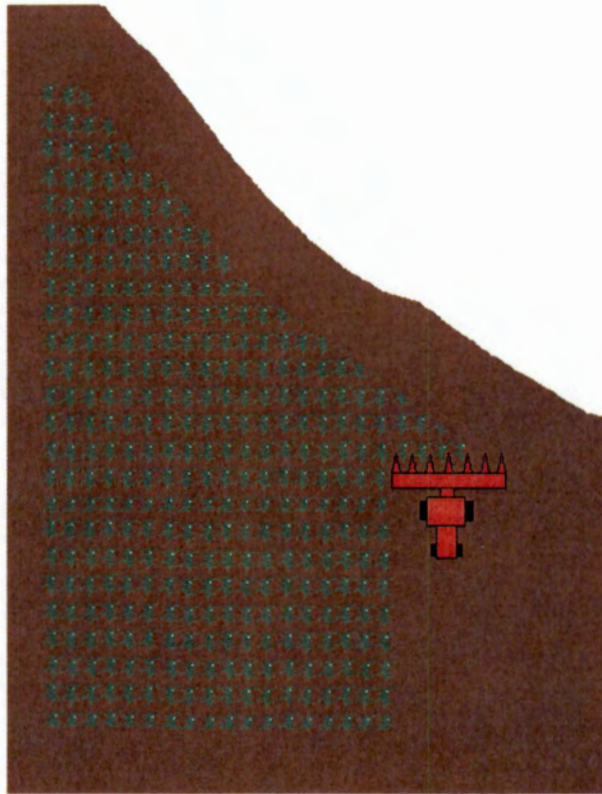


Figure 1. Combine harvesting point rows due to irregularly shaped field.

moved through the corn, stalks would push the rod back and rotate the potentiometer. The potentiometer is set such that when it rotates the potential changes. This change was fed into circuitry that processed the signal and recorded the count. A spring then returned the rod back to a mechanical stop at its original position to await the next stalk.

The sensor was field tested in transects approximately 10 m in length where the distance between each stalk and the number of stalks were known. Tests consisted of operating the sensor at three ground speeds (3.2, 5.6 and 8 km/h) with each test replicated four times. The sensor generated multiple high frequency pulses; therefore, filters were used

to reduce over counting caused from this and were somewhat helpful. After harvesting tests, the data was processed using 2 different filtering methods. In method 1, time windows of 11, 17, 23, 29, and 35 milliseconds were used to eliminate multiple counts occurring within each time window. In method 2, distance intervals of 2.5, 5.0, 7.5, 10.0, and 12.5 cm of actual field travel were specified to eliminate multiple counts that occurred within these distances. Both methods proved useful in reducing over-counting, with distance-based being more accurate. Birrell and Sudduth found that corn stalks closer together than 5 cm were only counted 50% of the time. The error resulted from the inability of the potentiometer to spring back from the previous plant quickly enough to measure the succeeding plant.

Birrell and Sudduth (1995) reported that the sensor accurately counted corn population at higher speeds (8.0 km/h), but overestimated the corn population at slower speeds. Heavy weed population was a major problem at low speeds; weed stems were repeatedly counted as corn stalks. The sensor did distinguish between feeding and idle rows. Their sensor could be used to sense row activity although corn population would not accurately be known.

Capacitive Method

A concept for counting crops at the corn head has been developed and patented by Stephen W. Nichols (2000). The sensing element used by Nichols was a capacitive proximity sensor commercially available (Effector Inc. model KB5004). Output from

this sensor is connected to a counter that increments every time a “moisture-containing product is located within the detection range” (Nichols, 2000).

The sensor is mounted on the cowl above the gathering chains in front of the snap rollers. A metal clamping device secures it to the cowl and a shroud is used for protection against stalk impacts. Figure 2 illustrates the sensor mounted on the cowl of a combine corn head. The sensor is a moisture sensor and “is not triggered by leaves or other debris as it passes by the moisture detector” (Nichols, 2000), since leaves and debris lack the moisture content to trigger the sensor.

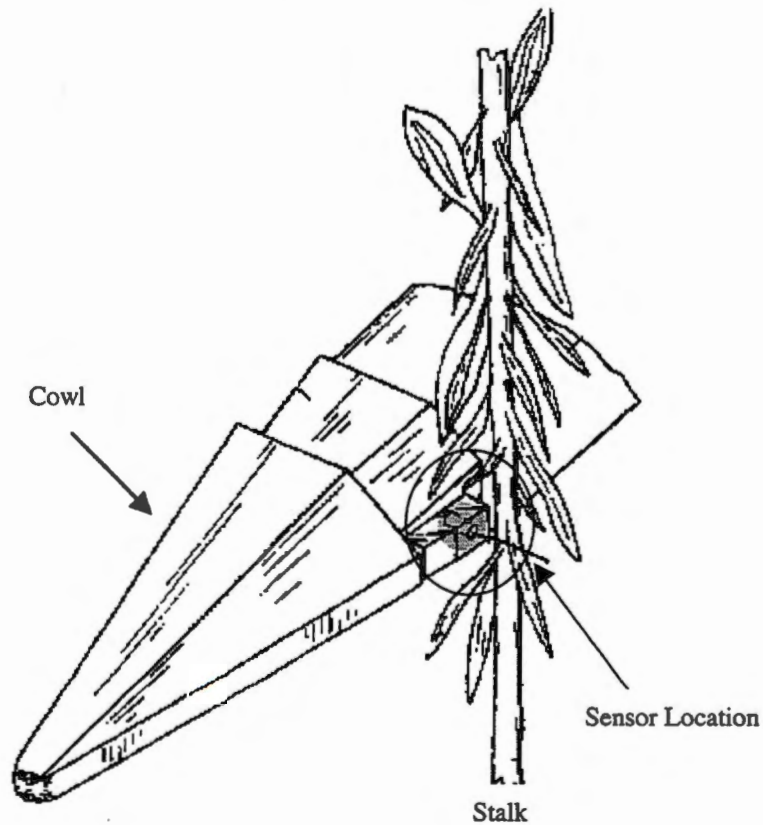


Figure 2. Mounting location of capacitance sensor (Nichols, 2000).

While the concept presented by Nichols is sound, several factors may limit the system's practical application. Stalks under certain conditions may not have enough moisture to trigger the sensor. Corn left in the field due to poor field conditions or bad weather may give the stalks time to dry out to unsensible moisture contents. Also, the sensing distance is limited and stalks could pass by without being detected if they are against the other side of the cowl. A review of literature reveals no laboratory, or field test information regarding a capacitance sensor used to measure corn population.

The sensor described in the patent was obtained and evaluated in the laboratory. It was determined that limitations on range and sensible stalk moisture content make the sensor unsuitable for its intended use. This is addressed in detail in chapter 4. The decision was made to develop a sensor well suited to the task described by Nichols. Testing and further development of the concept are described below.

Theory Behind Capacitance

As with many electrical concepts, most people find capacitance hard to understand because electricity is generally invisible. This is unfortunate since capacitance is easily understandable after a short analysis. The simplest capacitor form is two parallel plates with a dielectric material separating them as illustrated in figure 3. When the capacitor is energized, one plate has positive charges and the other has negative charges that cannot cross the dielectric material (Rizzoni, 1996). The ratio of charge to voltage is called capacitance, and is determined by the following equation.

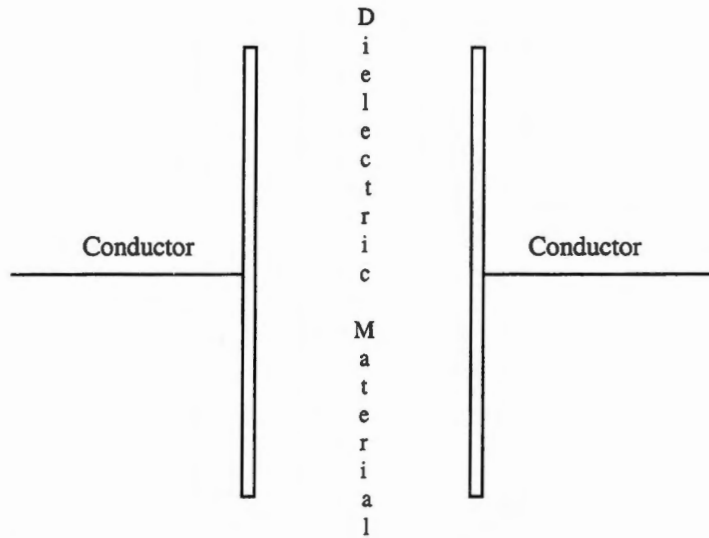


Figure 3. Dielectric material separating 2 parallel plates.

$$C = \frac{q}{v}$$

Equation II

where C = the capacitance (Farads)

q = charge (coulombs)

v = potential (volts)

The unit of capacitance is the Farad; however, one Farad is an extremely large unit, thus picofarads ($1\text{pF} = 10^{-12}\text{ F}$) and microfarads ($1\mu = 10^{-6}\text{ F}$) are often used to express capacitance.

No current flows in a capacitor as long as the potential remains constant. Because of this a capacitor acts as an “open circuit in the presence of DC currents”. However, if the voltage across the capacitor plates changes over time, the amount of charge will also

change causing current to flow into and out of the capacitor (Matsch, 1964).

Unlike a resistor, which converts all absorbed energy into heat, a capacitor is an energy storage device that holds potential energy on charged conductors separated by a dielectric. This stored energy can be completely recaptured in an electric form (i.e. No power is dissipated). The amount of energy stored in a capacitor can be expressed as follows.

$$W = \frac{Cv^2}{2} \quad \text{Equation III}$$

where W = energy (joules)

C = capacitance (Farads)

v = potential (volts)

Storage capacity depends on the electric field capacity of the plates (Matsch, 1964). A dielectric is a non-conducting material that becomes polarized in the presence of an electric field (Rizzoni, 1996). The dielectric's property is usually expressed as a relative dielectric constant, which is based on the electric permittivity of a vacuum. All materials have unique relative dielectric constants, with water having the highest (87) and a vacuum having the lowest (1) (Baxter, 1997). If the electric field exceeds the dielectric's capacity, the dielectric will break down, discharging the capacitor. An example of this break down is a bolt of lightning which is created when the electric field density in air exceeds three million volts per meter (Matsch, 1964).

With the definitions of capacitance and dielectrics known, a more simplified equation for a parallel plate capacitor can be given. If the relative dielectric constant

between the plates is known and the fringe flux lines at the edge of the plates are ignored, the expression for capacitance can be simplified to the form seen in equation IV.

$$C = \frac{\epsilon_0 \epsilon_r A}{d} \quad \text{Equation IV}$$

where C = capacitance (Farads)

$\epsilon_0 = 8.854 \times 10^{-12}$ (Electric permittivity of vacuum, Farads/m)

ϵ_r = relative dielectric constant

A = area of one plate (m^2)

d = distance between plates (m)

This equation is only useful for parallel plates; however, many other equations have been derived for other capacitor geometries.

Capacitance Sensors

Some capacitance-based proximity sensors have a conductive sensor head which acts as one plate. The object being sensed is conductive and grounded, and it acts as the other plate. An air gap is present between the sensor head and object to insure that when the grounded object passes in front of the sensor head there is a magnitude increase in capacitance due to air having a low dielectric constant (Warring and Gibilasio, 1985). The object's ground state causes the sensing head to extend its field outwards towards the object and the object is sensed due to the difference in potential (Dally, et al., 1993).

Figure 4 illustrates this concept for interactions of the fields.

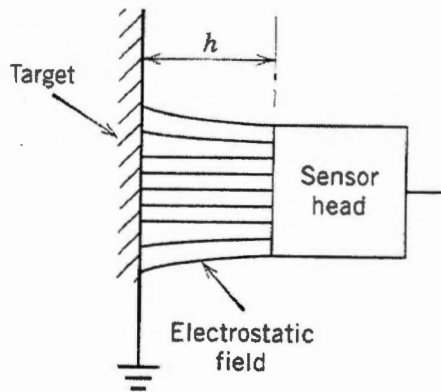


Figure 4. Field lines of single plate capacitor (Baxter, 1997).

An oval is the simplest and most basic sensor head configuration. The oval's size is a predictor of how far the sensing distance will be to the target object. Capacitance of this sensor can be determined with equation IV where the area of the sensor head replaces the area of the plate. A good rule of thumb is to take the sensor head diameter and divide by four to get the limit of the sensor's range. Likewise, the sensitivity is reduced the larger a sensor becomes (Dally, et al., 1993). Sensitivity can also be increased by incorporating a guard ring around the sensor head to keep stray electrostatic fields and fringe fields under control, and in doing so increases the approximate range to the diameter divided by two (Dally, et al., 1993). Fringe fields are distorted field lines along the edge of the sensor. As illustrated in figure 5 the guard helps focus the sensor field and does not have to be at the same potential as the sensor head. It can be at any DC or AC voltage and the result will be the same (Baxter, 1997).

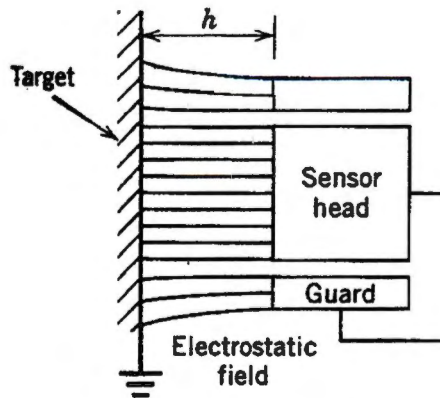
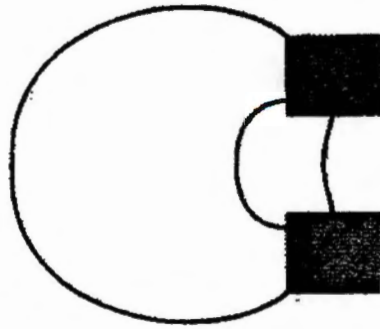


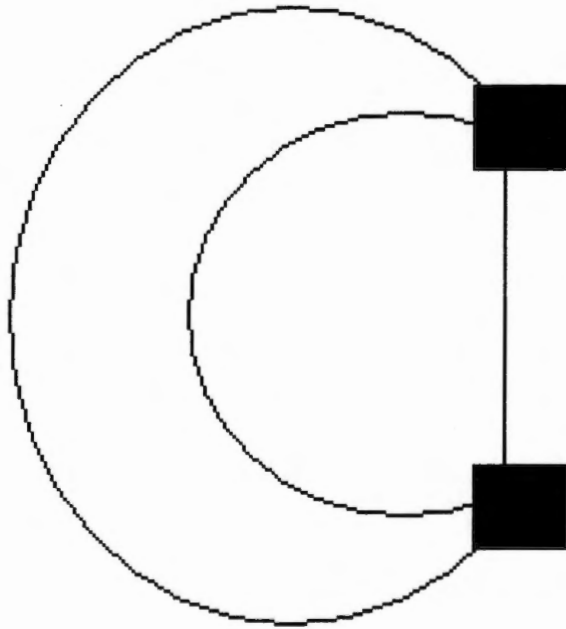
Figure 5. Capacitance field lines being focused with guard ring (Baxter, 1997).

Proximity sensors can be taken a step further by using the guard ring as another electrode with the sensor head electrode. In this configuration, one electrode acts as one plate of the capacitor and the other electrode acts as the other plate. Capacitance sensors of this type depend on fringe fields that occur between the 2 electrodes for their sensing ability. The object being sensed no longer has to be grounded or conductive because the sensor is totally dependent on fringe fields (Chen, et al., 1996). Figure 6 shows electric field lines that occur between 2 electrodes. The closer the 2 electrodes are together the stronger the electric field. The strongest and most sensitive fields are located close to the face where the fringe field arcs are shorter (Baxter, 1997). The range of this type of sensor can be anywhere from a few inches to a few thousandths of an inch (Chen, et al., 1996).

Sensors described above all depend on the ability to measure change in capacitance. Several techniques have been developed to make these measurements (Warring and Gibilasio, 1985). Baxter (1997) described one type of a single-ended



(a)



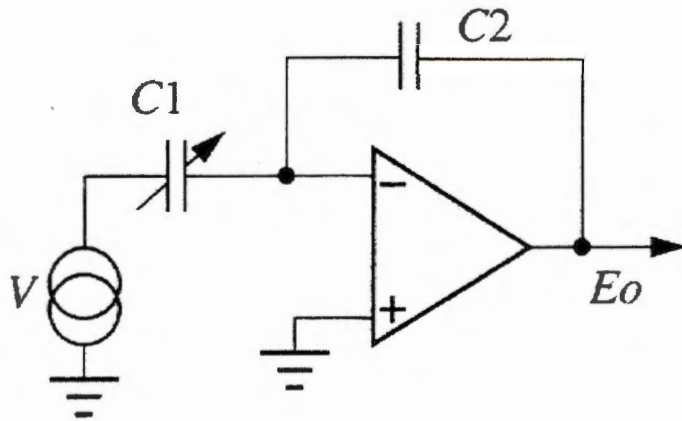
(b)

Figure 6. Capacitance fringe field lines as a function of distance. (a) Electrodes close to together and (b) electrodes farther apart (Baxter, 1997).

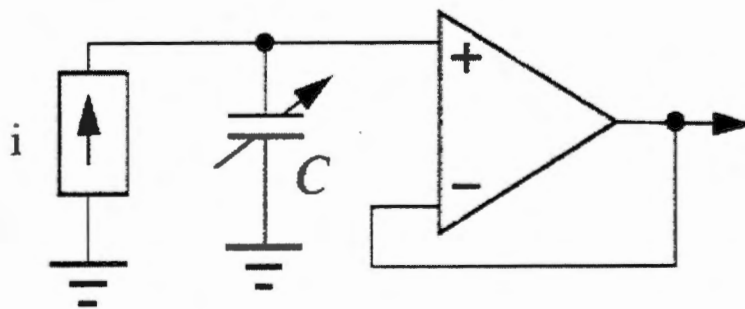
circuit that uses a discrete capacitor, such as a mica or film dielectric component, as a reference (Baxter, 1997). See figure 7a for one example of a single-ended measurement circuit. This circuit makes use of a low impedance amplifier or virtual ground amplifier. The feedback capacitor is the discrete component. An alternating voltage source connects to one electrode of the sensor and the other electrode is connected to the negative input of the amplifier. This gives an output equal to the excitation voltage times the ratio of the sensors capacitance to the feedback capacitor. The use of a capacitor as a feedback element improves noise performance by removing real components from the system (Baxter, 1997).

Another measurement configuration is shown in figure 7b. This circuit includes a high impedance amplifier used in a non-inverting amplifier configuration. This technique does not use a discrete reference capacitor as the feedback capacitor. Instead, an AC current source is used as the reference for the system. The sensor has one electrode grounded and the other connected to the AC source and amplifier. When the sensor capacitance changes, more or less of the AC current is taken to ground. Because of this, the output is proportional to the impedance of the sensor (Baxter, 1997). Both of these methods are highly unstable if not shielded from stray capacitance, and make measurement of very small changes in capacitance difficult.

A bridge circuit on the other hand is very stable under these conditions, and is useful for measuring small changes in capacitance. When a bridge is excited with a high frequency waveform of 100 kHz or more it can easily measure a change in capacitance to a few parts in a million. The high frequency waveform reduces the impedance of the



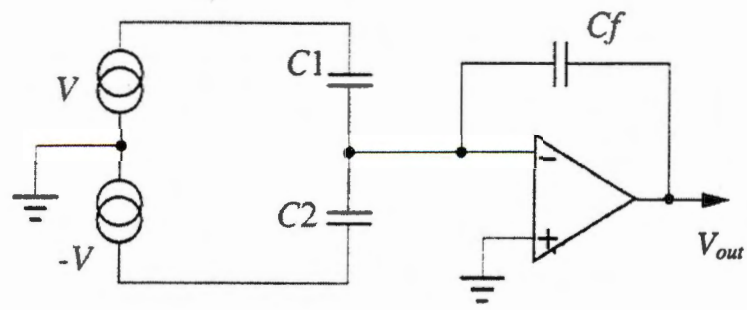
(a)



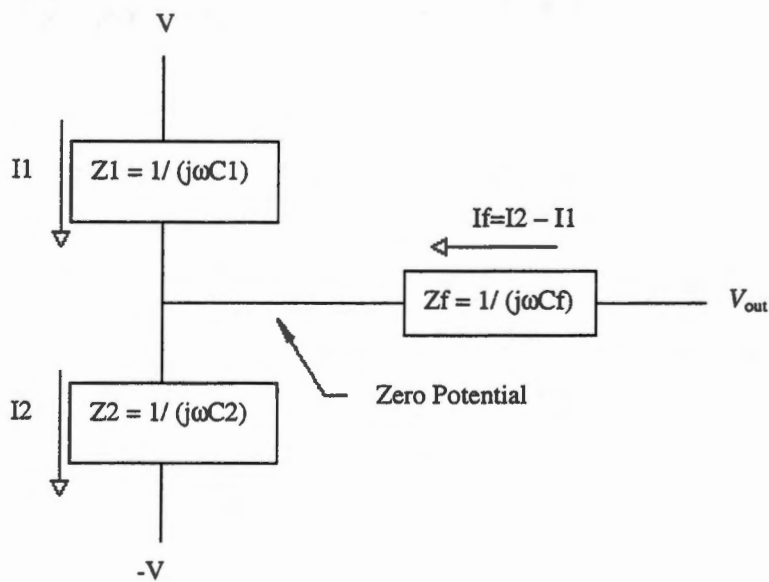
(b)

Figure 7. Single-ended capacitance measurement methods. (a) low impedance amplifier, and (b) high impedance amplifier.

sensor from the megohm range to the kilohm range, which results in an increase in sensitivity (Baxter, 1997). The leg of the bridge should be constructed of components that are made of similar materials. That makes stabilizing the bridge much easier since similar component temperature changes will track one another. The output is also insensitive to power supply and other circuit variations that would cause single-ended circuits to have DC error present on the output. One form of a capacitance bridge can be seen in figure 8a. The bridge is single-legged with a reference capacitor and sensor connected in series. The bridge is driven by a balanced drive producing oscillations 180 degrees out of phase (Baxter, 1997). The output formula is derived as follows and can be seen visually in figure 8b. The amplifier connected to the bridge is in the virtual ground configuration. This means that feedback current will flow through the feedback capacitor C_f such that the (-) amplifier input will be at zero potential. This, along with Kirchoff's current law, and the assumption of no current flow into the amplifier input allows simple analysis. Total current through the feedback capacitor can be calculated by knowing the current through the 2 capacitors on the bridge leg. Knowing the feedback current, referred to as I_f in figure 8b, and the impedance of the feedback capacitor provides the output voltage from use of ohms law. The final equation can be seen in equation V.



(a)



(b)

Figure 8. Capacitance bridge measurement circuit. (a) Schematic of Capacitance Bridge and (b) visual interpretation of bridge output formula.

$$V_{out} = -V * \frac{C1 - C2}{Cf}$$

Equation V

where V_{out} and V = volts

$C1$, $C2$, and Cf = capacitance (Farads)

A review of the literature revealed no laboratory, or field test information regarding a capacitance sensor used to measure corn population. Testing and further development of a capacitance based sensor are described herein.

Chapter 3--Sensor Design & Evaluation

Design Background

Two sensing techniques were investigated during the course of this development effort. The original prototype sensor was an intrusive piezo-electric impact sensor. Piezo-electric film was chosen because of its high sensitivity and reliable force measurement capability. During field-testing, serious problems were discovered. The intrusive nature of this design results in many stalks being knocked over. This is due to deteriorated root systems late in the year. Also, multiple stalks in contact with the sensor simultaneously greatly dampened the sensor sensitivity. Because of the destructive nature of the impact sensor, it was abandoned in favor of a non-intrusive technique. The final prototype was a capacitance proximity sensor. This device detects changes in dielectric properties of adjacent material and produces a voltage output. The sensor consists of a brass ring and disc that depend on fringe fields for sensing. Laboratory and field-testing proved this design is capable of counting corn stalk population.

Impact Sensor Design

An impact sensor was designed, prototyped, and tested. A pre-fabricated strip of piezoelectric film (Measurement Specialties DTI-028K/L) was used for the sensing element. The film selected was 2-inches by ½-inch with a sensitivity of $400 \times 10^{-3} \text{ V}/\mu\text{m}$. Piezoelectric film is comprised of two layers of material overlaid on each other. When the film is impacted the two materials rub against one another, creating a voltage. Voltage

output is proportional to the rate of change of relative velocity of the two materials rubbing together (Dally, et al., 1993). A prototype sensor was designed to be rugged, yet highly responsive to corn stalk impacts. A mounting technique was designed to provide protection for the film without compromising dynamic response. After testing several materials and geometries, it was determined that piezo-electric film bonded to the back of a thin titanium band (0.625 x 5.125 x 0.035 inches) bent to form an arc provided the dynamic precision and durability required. The titanium band was mounted to a wedge-shaped aluminum block (2.25 x 3.00 x 2.38 inches) illustrated in figure 9(a). Space between the band and block was filled with silicon to prevent trash from accumulating. Because stalks have varying diameters, two sensors were mounted opposite each other on a row unit, (figure 9 (b)), to prevent stalks from passing unsensed. Sensor blocks were adjusted such that small-diameter (0.75 inches) corn stalks would be sensed, while still allowing enough clearance to permit larger diameter stalks (1.5 inches) through.

Laboratory Test Equipment

A stationary stand was designed and built for laboratory testing of designs in controlled environments. A photograph of the test stand is seen in figure 10. The test stand consists of a wheel driven by a variable speed DC electric motor. The wheel is composed of two pieces of ½-inch PVC sheet, 20 inches in diameter, sandwiching a smaller PVC piece creating a 2-inch gap between the outer pieces. Test materials are placed in this gap and secured by bolts to prevent movement during testing. The PVC wheel is supported by a cross member adjustable in the vertical plan to position mounted

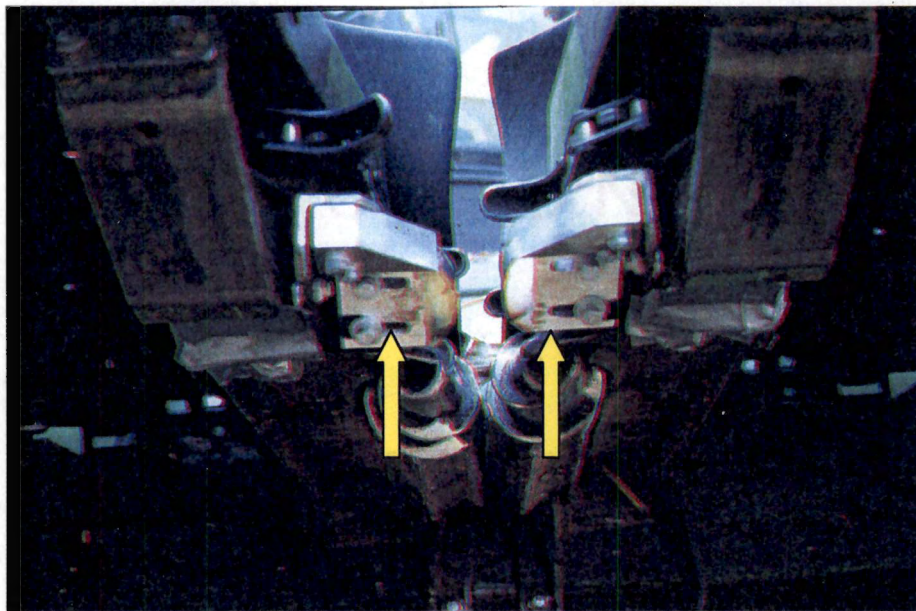
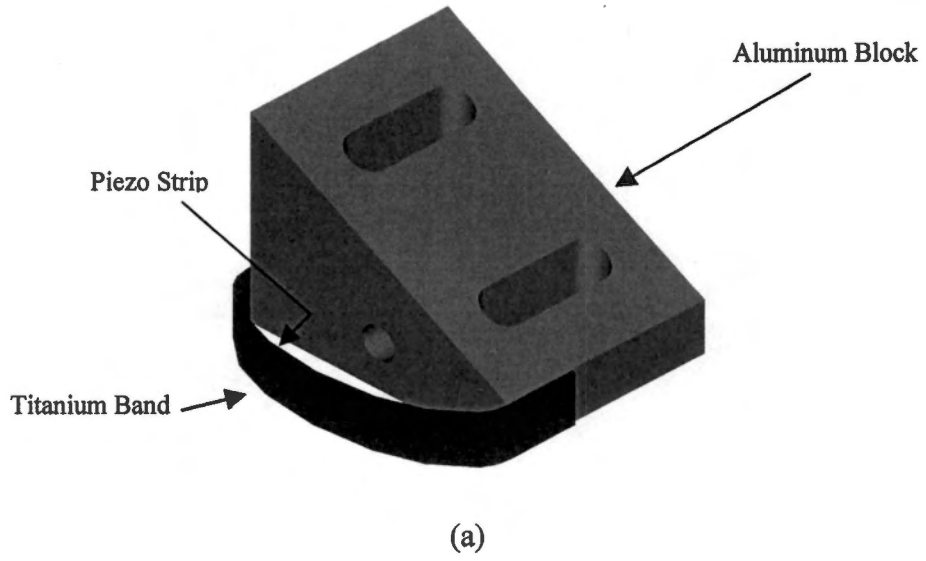


Figure 9. Pictorial representations of impact sensors. (a) Conceptual design of impact sensor, and (b) placement of impact sensors on combine row unit.

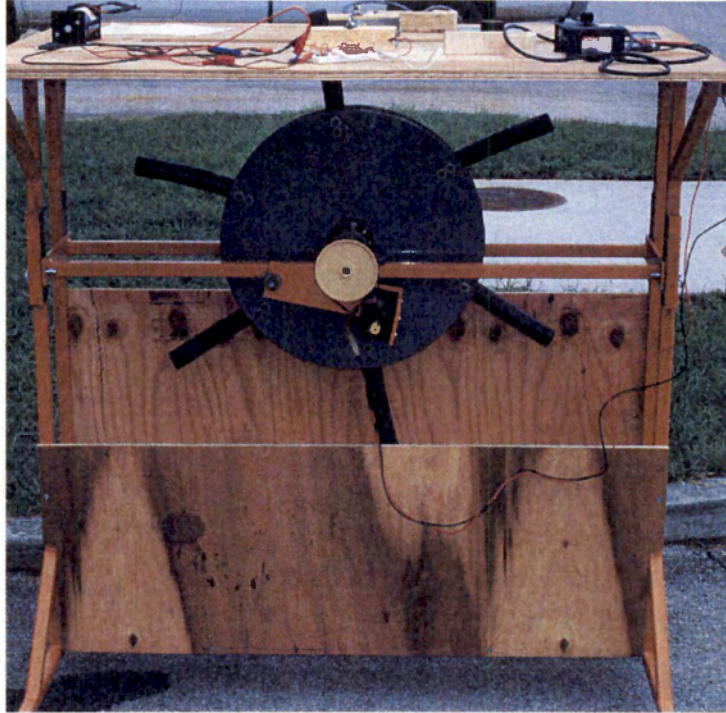


Figure 10. Test stand used to evaluate sensor designs under controlled conditions.

materials within sensing range of sensors on the tabletop. A slot is present in the stands tabletop and allows test materials to rotate through the top. This slit is the width of the gap present on a combine row unit where the sensor is mounted to simulate in-field conditions. Effective operating speeds of 0.6 to 3.0 mph (11.25 to 44 RPM) can be achieved using the variable DC motor with 1:8 timing gear drive reduction.

Laboratory Testing

Lengths of cylindrical rubber stock (1.25 inches dia.) were mounted to the test stand wheel, and used to impact the sensor face. The resulting waveforms were captured on a digital storage oscilloscope (Tektronix TDS3014). Results from this test provided

information indicating that waveform amplitude was substantially higher than base line noise upon impact. This was essential in determining if the sensor could produce signal levels high enough to overcome signal noise due to vibrations on the combine corn header. A sampling rate of 5000 Hz for data acquisition was based on simulated ground speed of 4.0 mph and stalk diameter of 1 inch.

Field Test

Results from the first field test, conducted in August 1999 at Milan Experiment Station, were very informative. As expected, weeds, leaves and other material did not affect sensor output. However, the sensor had problems distinguishing between stalks when stalk spacing was less than 3 inches. Specifically, when stalk spacing was less than 3 inches, a stalk was always present on the sensor face. Thus, when another stalk impacted the sensor, the previous stalk on the face dampened the impact of the incoming stalk, reducing the signal-to-noise ratio.

To address this issue, the two sensors were rotated (15°) to minimize the face area present for an impact. The system was tested again in November, 1999. However, during this test, another problem arose. Due to the length of time stalks had been in the field, stalk root systems had deteriorated. Thus upon impact with the sensor, stalks were pushed over and not harvested. This problem was so severe, the decision was made to abandon impact sensor development in favor of a non-intrusive technique.

Capacitance Based Sensor Design

Design Overview

The prototype capacitance sensor face is comprised of a brass inner disc and brass outer ring. This type of capacitance sensor is based on fringe fields for its ability to sense objects. Gap distance between the disc and ring determines the sensitivity. Thus, the smaller the gap between the disc and ring the more sensitive the sensor becomes (Chen, et al., 1996). The sensor has the ability to sense corn stalks from air due to a change in dielectric constant. The ring and disc produce an electric field that is affected by the presence of a dielectric material causing a change in the capacitance that can be measured (Baxter, 1997).

The prototype system consists of a sensor, half bridge, high-pass filter, demodulator, amplifier, and signal-processing block which is implemented in software. Figure 11 illustrates system components using a block diagram. The sensor is a capacitance proximity sensor that is connected along with a reference capacitor in a half bridge. When the bridge becomes unbalanced a voltage is produced as described in chapter 2. A high-pass filter is connected to the bridge and allows frequencies greater than 66 kHz to pass. The signal is demodulated in the next stage to produce a DC signal. The final stage is amplification to provide a low-impedance, high signal-level output.

Signal processing is conducted in software. A low-pass filter is applied to the data to eliminate noise and smooth the waveform. Application of a derivative function produces peaks whenever the slope is large. Steeper slopes produce peaks with higher

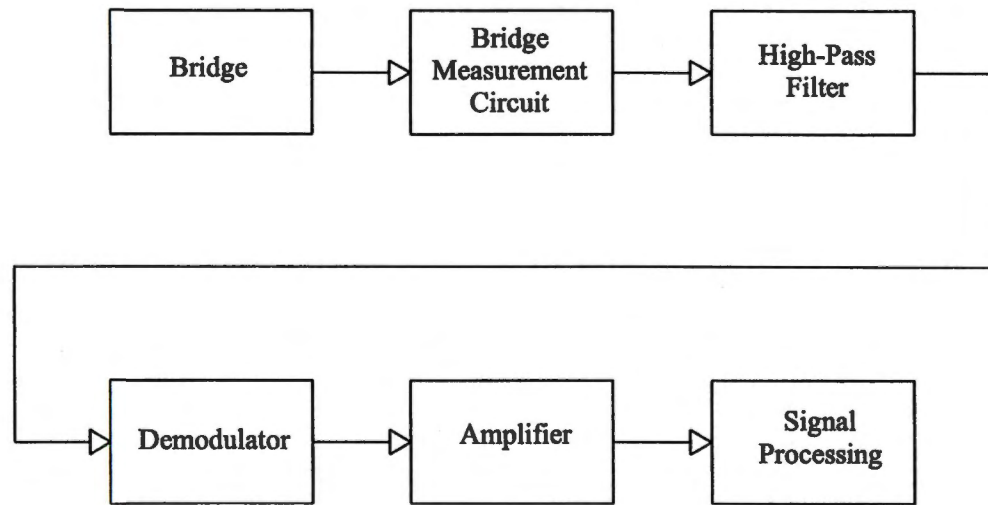


Figure 11. Block diagram of system components.

magnitudes than small slopes. Data is then smoothed again with another low-pass filter. A hysteresis function is applied to insure that multiple counts do not occur due to jagged waveforms. One corn stalk can only occur within a certain number of samples. Thus, each stalk count is examined to determine if it spans more or less samples than possible. If more or less stalks are present than first determined the count is incremented to account for this. The final stalk tally is then recorded.

Sensor Head and Mounting Bracket Design

Refer to figure 12 throughout this section for an assembly drawing of head and bracket (Appendix A for mechanical drawings). The sensor face consists of an inner disc (1.75 inch dia.) and outer ring (1.875 inside and 2.25 outside dia.) that are fabricated from brass shim stock (0.050 inch thick). The gap between the inner disc and outer ring was 0.0625 inch. As discussed in chapter 2, sensitivity is increased the closer the ring and disc are together; however, sensing distance is sacrificed for sensitivity. Disc area was increased to obtain the desired sensing distance of 1.5 inches, while maintaining maximum sensitivity. Sensing distance was determined experimentally in the laboratory to be 1 inch with this configuration. A circular geometry was chosen because the fringe fields are equal strength around the face providing a constant output as a stalk passes.

The brass disc and ring are recessed into a polyvinyl chloride (PVC) head, and are covered with a piece of lexan to prevent the disc and ring from being shorted or grounded through inadvertent contact with an object. The head-mounting bracket is designed to mount on the combine corn head cowl as close to the snap rollers as possible while

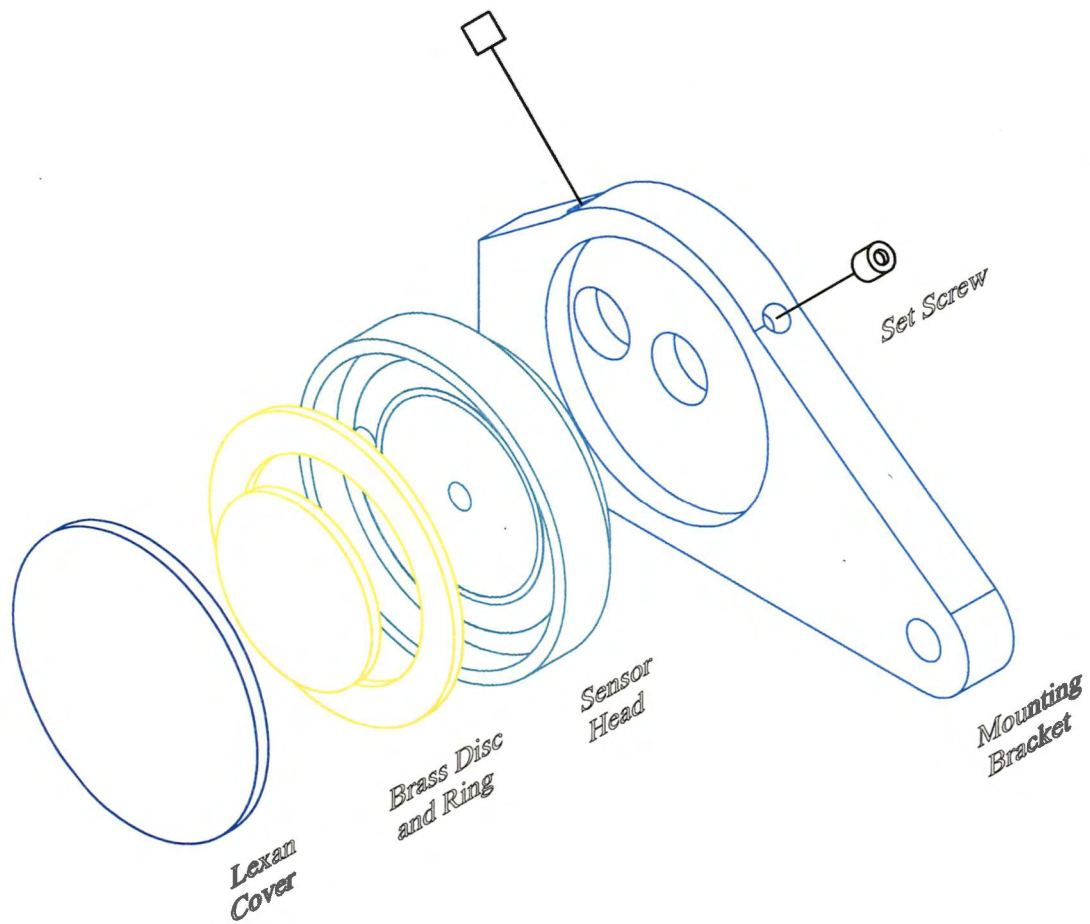
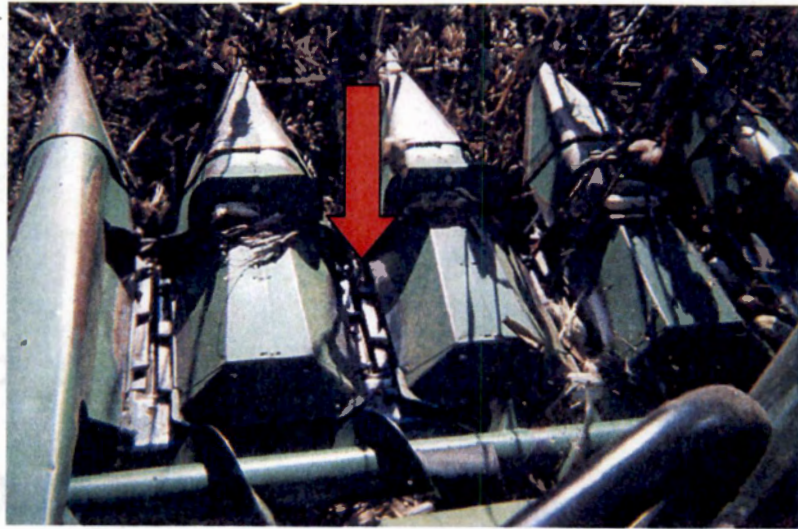


Figure 12. Assembly drawing of sensor head and bracket assembly.

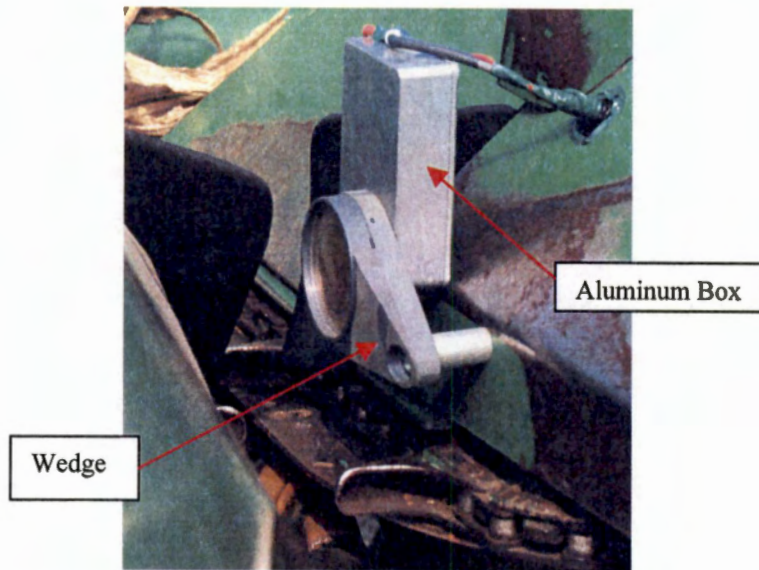
providing protection for the head from incoming stalks (figure 13(a & b)). This is the optimum placement for the sensor because the throat of the row unit keeps stalks within 0.75 inches of the sensor face. Also, a wedge (figure 13b) was designed into the side of the bracket that faces the incoming corn stalks to provide sensor head protection. The sensor mounting-bracket is machined to allow the sensor head to fit into it, and the head is held in place with hex key set screws. These set screws allow the head to be easily removed and replaced with different electrode geometry if needed. A cast aluminum enclosure (4.72"x3.15"x2.17", Hammond Manufacturing), illustrated in figure 13b, is mounted opposite the sensor head to provide storage for signal processing circuitry. Holes drilled through the bracket, box, and head allow wires to connect circuit board to sensor electrodes.

Signal Processing Hardware

Recall that a detailed discussion of the measurement of the head capacitance is described in chapter 2. In short, the dielectric surrounding the sensor head increases in the presence of an object with a dielectric constant greater than air, thus causing the bridge to become unbalanced. As shown in Chapter 2, the output of the bridge is related to the change in the impedance of bridge components. The bridge is manually balanced when no objects are present by adjusting a tuning capacitor on the leg of the bridge. However, a DC bias is present on the output of the bridge because a small resistive component exists on the tuning capacitor. This results in a DC offset in the bridge output. This bias has to be lowered to prevent the next stage amplifier from being “taken to the rail” and



(a)



(b)

Figure 13. Mounting location of capacitance sensor. (a) Row unit sensor was mounted to with arrow indicating 3rd row, and (b) mounting location on cowl.

damaged. "Rail" is the maximum working voltage allowed by the amplifier design and is based closely on the supply voltage of the amplifier. To reduce the output offset voltage, a resistor is placed between the non-inverting input of the amplifier and ground. This feature, along with a small amount of input current, supplies a reference point for the amplifier other than ground. Reference voltage supplied by leakage current, in combination with the resistor lowered system bias slightly; however, it was still present.

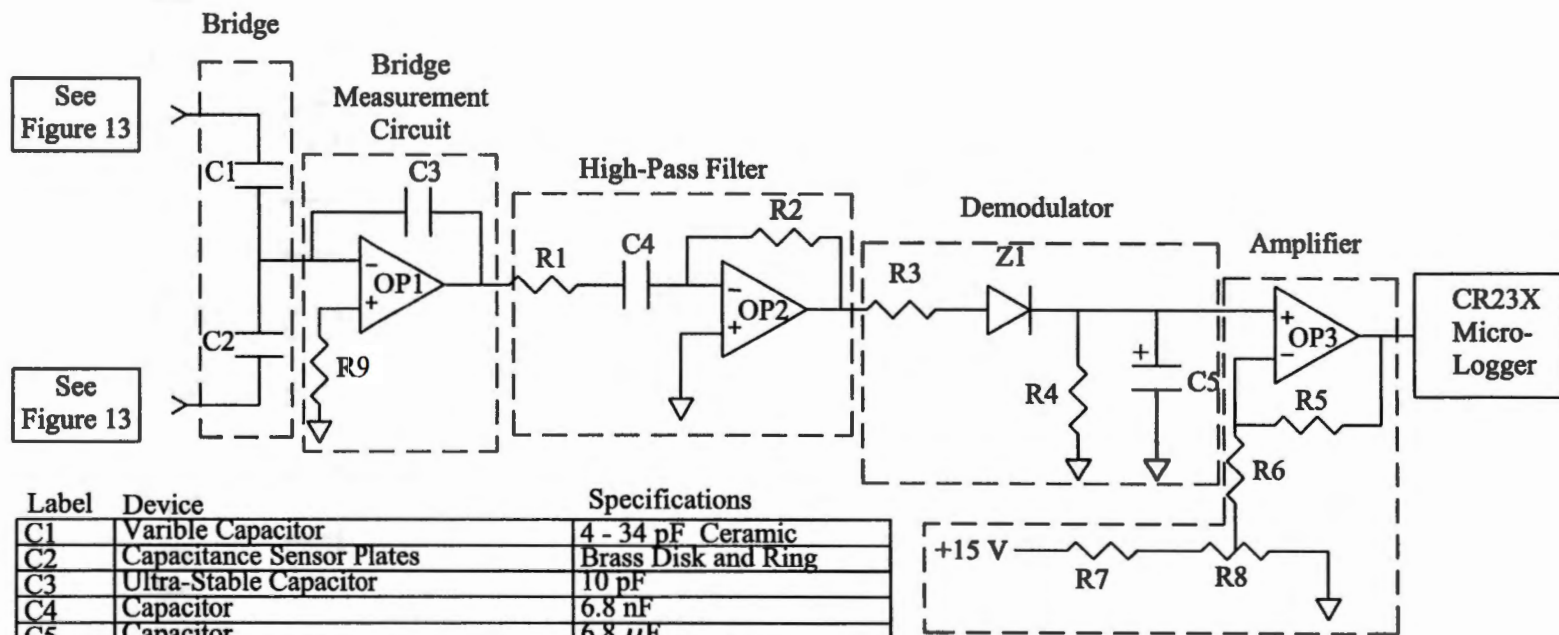
The output of the amplifier is passed through a high-pass filter that has sufficient gain to increase the voltage so that the signal amplitude is not greatly affected by the 0.4 voltage drop through the high-pass diode. The filter negates the presence of a DC bias, and attenuates all frequencies less than 66 kHz.

Output of the high-pass filter is rectified with a single diode. This diode provides half-wave rectification so the negative component of the signal is negated. An electrolytic capacitor is included and sized such that ripple is minimized without increasing system response time. A resistor is connected prior to the diode to prevent feedback from occurring between the electrolytic capacitor and the output of the high pass filter. Finally a resistor to ground is connected after the diode to load the signal enough to ensure proper rectifier operation.

After rectification, a non-inverting amplifier is used to amplify the signal so that even the most minuscule change is noticeable. However, the signal feeding into the operational amplifier is at some positive value because of offset present at the beginning of the circuit. Therefore to prevent the signal from going to the rail when an object is sensed, a voltage divider is connected on the reference leg of the amplifier. The voltage

divider has a variable resistor that can be adjusted to add a DC bias to the amplifier so that it can be zeroed. If a 5V output was present with nothing sensed, the variable resistor could be tuned and the voltage zeroed. With the output zeroed, the amplifier can swing between zero and the rail. Output is now ready to be connected to the data acquisition system. A circuit schematic can be seen in figure 14 and device specifications are included in Appendix B.

High-speed operational amplifiers are used throughout the circuit because of the extremely high frequency of 400 kHz. These high gains caused the operational amplifiers to have large swings in voltage from the input to the output. Standard operational amplifiers can produce only a finite rate of change in their outputs or slew rate problems occur (Rizzoni, 1996). Roll-off occurs when the frequency bandwidth of the operational amplifier is surpassed. When this occurs the signal begins to lose gain and the signal amplitude drops. To solve these problems high-speed amplifiers (LM 7171AIN, National Semiconductor) were installed that had extremely high slew rates ($4100 \text{ V}/\mu\text{s}$) and very wide bandwidths (200 MHz) for use in the circuit. Care had to be taken with these operational amplifiers to insure that they were not taken to their rails. If the signal ever reaches either rail it would begin oscillating back and forth between the rails, faster and faster, until the amplifier destroyed itself.



Label	Device	Specifications
C1	Variable Capacitor	4 - 34 pF Ceramic
C2	Capacitance Sensor Plates	Brass Disk and Ring
C3	Ultra-Stable Capacitor	10 pF
C4	Capacitor	6.8 nF
C5	Capacitor	6.8 μ F
OP1	Very High Speed Amplifier	LM7171 AIN
OP2	Very High Speed Amplifier	LM7171 AIN
OP3	General Purpose Amplifier	LM741 AIN
R1	Resistor	2.2 K Ω , 5%, 0.25W
R2	Resistor	4.3 K Ω , 5%, 0.25W
R3	Resistor	50 Ω , 5%, 0.25W
R4	Resistor	100K Ω , 5%, 0.25W
R5	Resistor	217K Ω , 5%, 0.25W
R6	Resistor	2.2K Ω , 5%, 0.25W
R7	Resistor	2.2K Ω , 5%, 0.25W
R8	Resistor	10K Ω Variable Resistor
R9	Resistor	10M Ω , 5%, 0.25W

Note: All chips powered by ± 15 Volts

Figure 14. Signal processing circuit schematic.

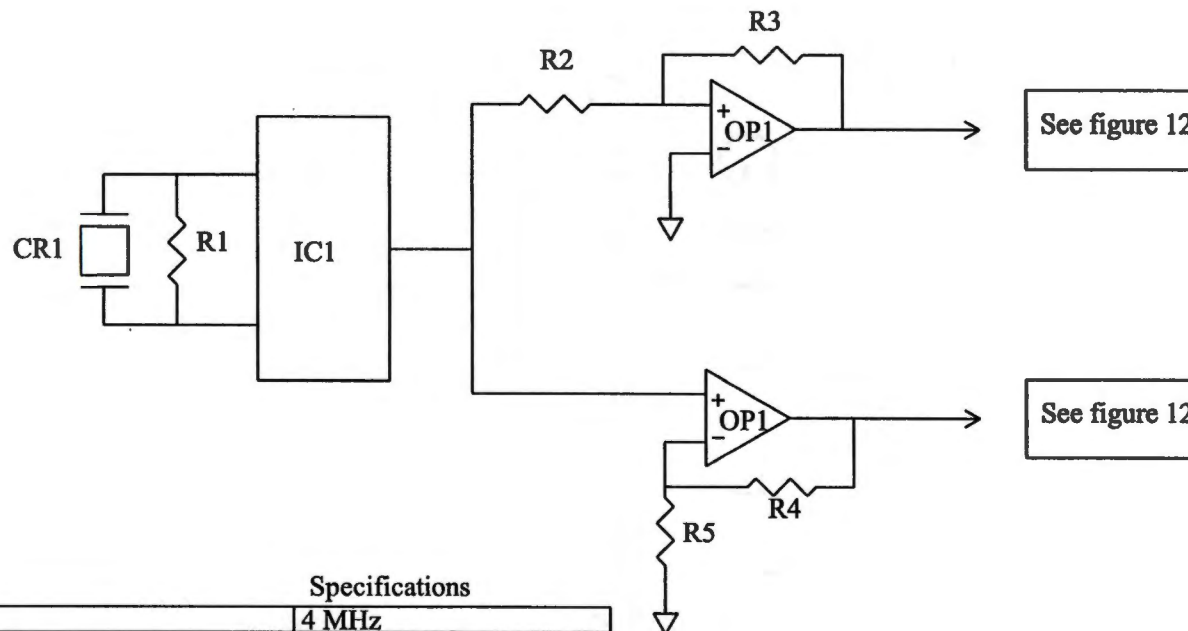
Frequency Generation

A frequency of 400 kHz is used because of the reduced sensor head impedance obtained from the high frequency. High frequency also increases sensitivity by increasing the difference between the dielectrics of air and biological material (Baxter, 1997). The 400 kHz frequency is the maximum design frequency for system components due to roll-off and slew rate limits of the circuitry.

The driving frequency for the system is produced with a 400 MHz crystal used in conjunction with a dividing integrated circuit (RDD104, LSI Corp). The RDD104, integrated circuit, divides a crystal's output by factors of 10, 100, 1000, or 10000. A 400 kHz square wave is produced using the integrated circuit divide-by-1000 option. This signal is connected to two analog devices (AD 823AN) operational amplifiers with bandwidths wide enough to handle the high frequency signal. Making one amplifier non-inverting and the other inverting causes the output difference between the two amplifiers to be shifted 180 degrees creating a balanced bi-polar drive for the bridge. Refer to figure 15 for circuit schematic.

Power Supply

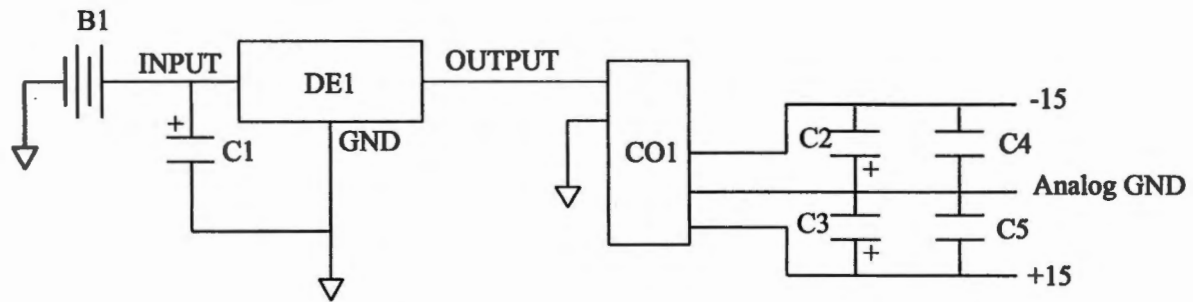
The signal-conditioning hardware requires voltages of ± 15 VDC. This voltage source is achieved by taking 12 VDC from a battery and supplying it to an LM 7803 (National Semiconductor) 12 to 5 V regulator. Regulator output is then supplied to a ± 15 V DC-DC converter (NMVO515S, Newport Components). Electrolytic capacitors are included to suppress power-supply noise. Power supply circuitry can be seen in figure 16.



Label	Device	Specifications
CR1	Crystal	4 MHz
IC1	Divide by 10	RDD104 (From LSI)
OP1	Dual, 16MHz Amplifier	AD 823 AIN
R1	Resister	10 M Ω , 5%, 0.25W
R2	Resister	3 K Ω , 5%, 0.25W
R3	Resister	5.1 K Ω , 5%, 0.25W
R4	Resister	2.2 K Ω , 5%, 0.25W
R5	Resister	3 K Ω , 5%, 0.25W

Note: All chips powered by ± 15 Volts

Figure 15. Frequency generation circuit schematic.



Label	Device	Specifications
B1	Battery	+12 V DC
C1	Capacitor	.22 μ F
C2	Capacitor	2.2 μ F
C3	Capacitor	2.2 μ F
C4	Capacitor	0.01 μ F
C5	Capacitor	0.01 μ F
CO1	Dual Output DC-DC Converter	NMH0515S (Newports)
DE1	DC-DC Converter	LM 7805 (National)

Figure 16. Power supply circuit schematic.

Data Acquisition System

A Campbell Scientific Inc. 23X micrologger and a Gateway 2000 Solo laptop computer were used for data acquisition. The micrologger's burst mode was used to rapidly sample data at a rate of 800 Hz. The data were written to final memory every 5000 points to avoid losing data since the burst mode's memory allocation was at capacity. It should be noted that the final memory storage transition takes 0.01 seconds, which translates to 8 missed samples. However, there should be approximately 233 samples per stalk; thus, no stalks should be missed during data acquisition. The program samples 5000 points, writes the data to final memory, and keeps repeating this process until it is stopped. A flow chart for the micrologger program is shown in figure 17, and the code is included in Appendix C. At the end of each test run the micrologger's sampling data was downloaded to the laptop and saved for later processing.

Data Post-Processing

All post-processing is carried out with programs written in MATLAB® (version 5.3, 1999) from The MathWorks Inc. A flow chart for the data-processing program is shown in figure 18, and the code is included in Appendix D. After the data is read from a file, a moving average is calculated. Five points are averaged and the value recorded into a new file. The next five points are chosen, and the process continues through all the data. This acts as a low pass filter, to smooth the data. Care is taken to not average too many data points or stalks might have been lost with a long averaging step. Refer to figure 19(a) for an example smoothed data graph. After the data is smoothed a derivative is applied to

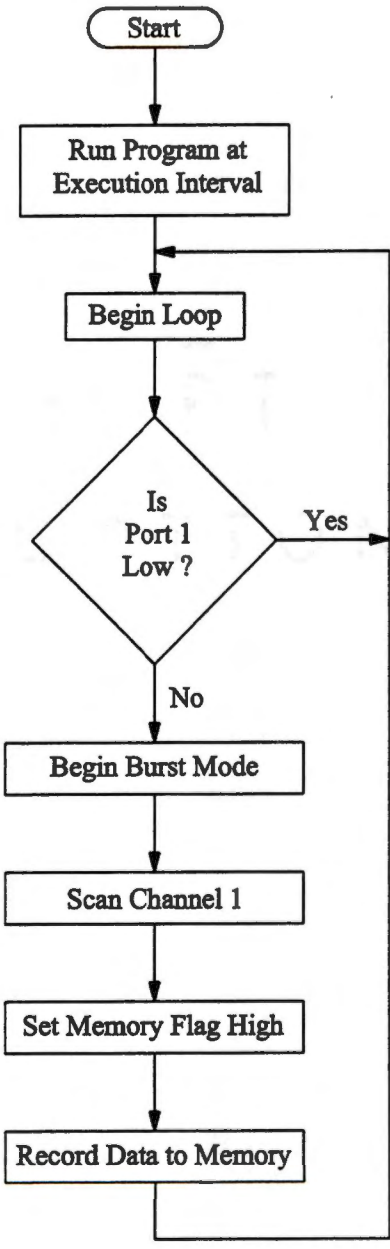


Figure 17. Flow chart of micrologger program.

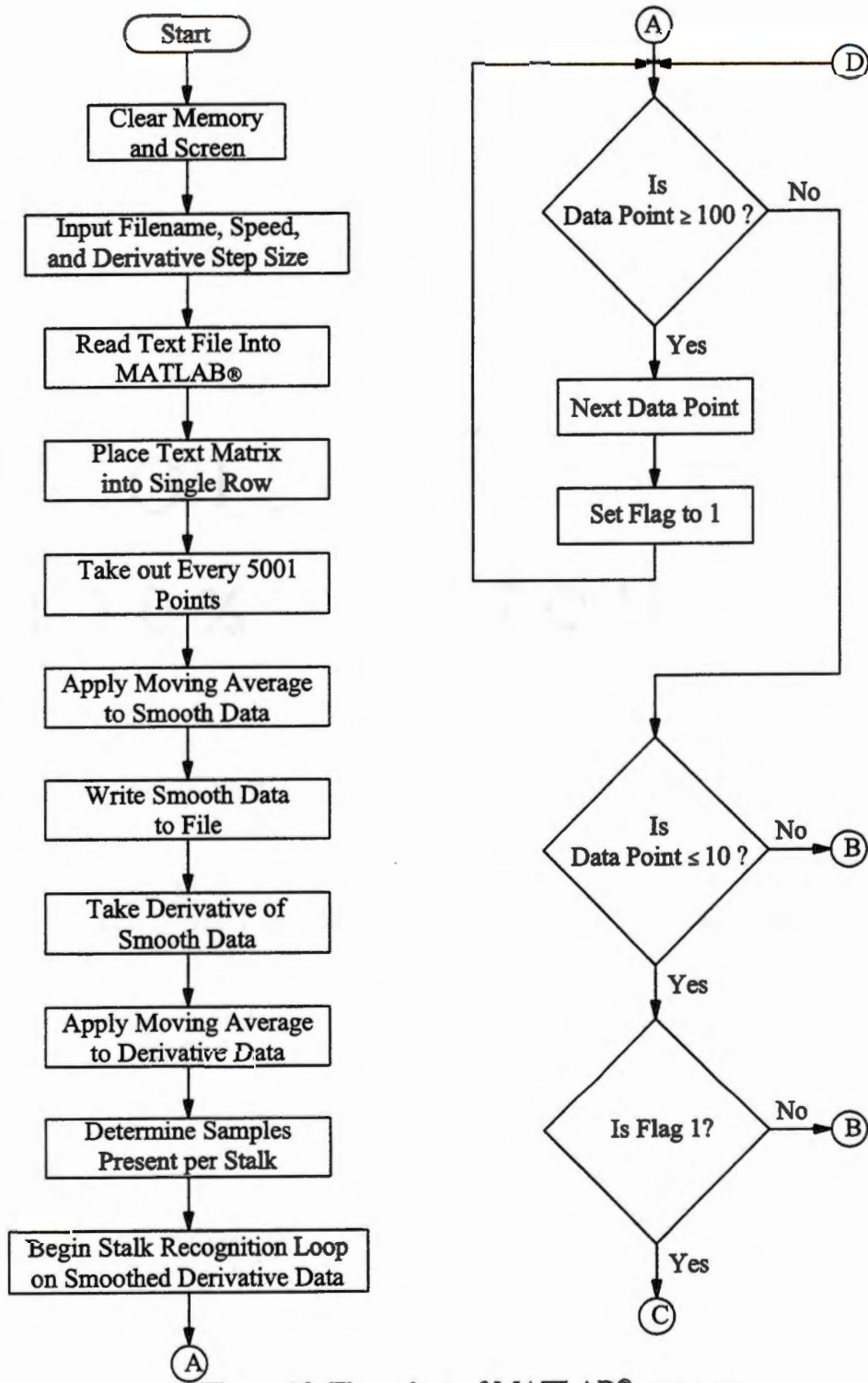


Figure 18. Flow chart of MATLAB® program.

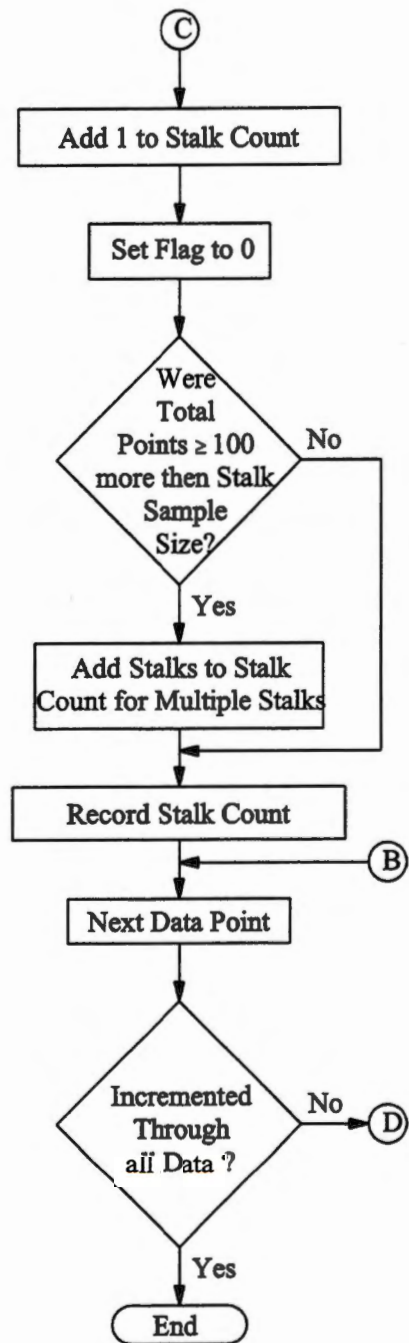
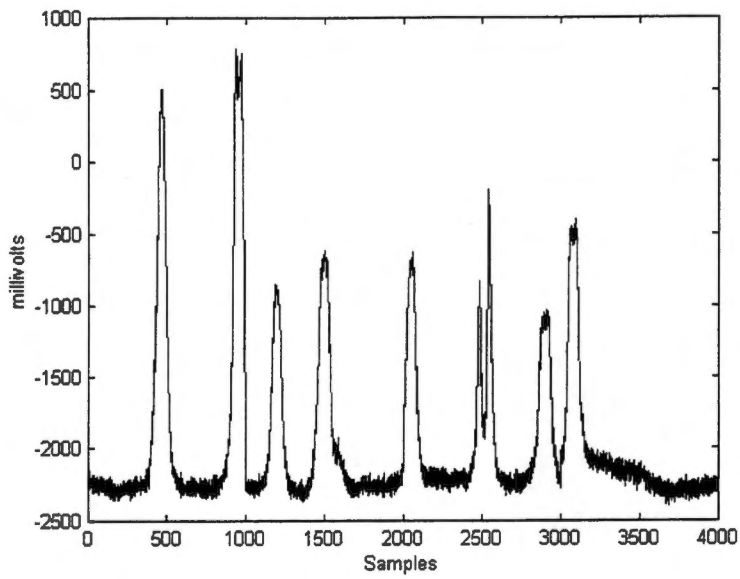
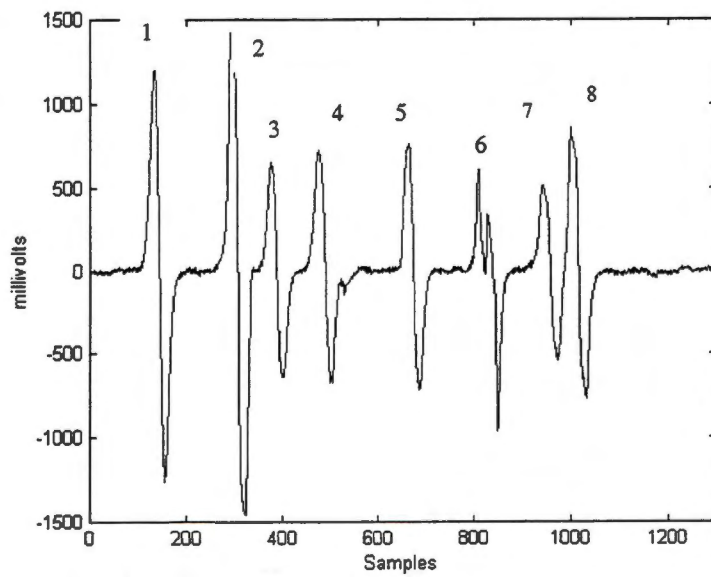


Figure 18. (Continued)
Flow chart of MATLAB® program.



(a)



(b)

Figure 19. Graphs illustrating data processing steps of 8 stalks at 0.4 mph. (a) Original data after being smoothed, and (b) smoothed derivative data.

exaggerate all severe changes in slope which represent corn stalks. This is accomplished by finding the difference between 2 data points using a step size of 30 (0.1875 seconds). The program looks at the 30th data point ahead and behind the current data point. The program records this and moves on to the next data point to perform the derivative again. A moving average is passed through the derivative data to further smooth it before the stalks are summed. The derivative of a signal is very sensitive to “noise”. When comparing figure 19(b), graph of derivative, to figure 19(a), it is easily observed that when there is a severe change in the averaged data’s slope there is a spike in the derivative for both the positive and negative slopes. Tallying of the stalks is accomplished by counting the peaks of the smoothed derivative data. Smoothed derivative data is used to insure that multiple counts do not occur due to noise on the waveforms. A count is recorded only after a waveform passes a maximum range (100 mV) and then drops back below a minimum range (10 mV) (hysteresis function). Multiple stalks can occur within this range so the program determines the maximum sample size for a stalk from machine ground speed and the sampling rate used, and uses this to calculate if multiple stalks are present in the hysteresis range. Finally the stalk count is incremented and the program moves to the next peak.

Laboratory and Field Testing

Field Test Equipment

For field-testing, the prototype sensor was mounted on a tractor-mounting bracket and corn header of a John Deere 4425 combine. The tractor-mounting bracket, illustrated

in figure 20, was used to obtain replications of data before the combine harvested the field. Replications were made before running the combine because of its destructive nature. The tractor-mounting bracket was designed to accurately position the sensor face a defined distance away from the stalk, and at approximately the same height as mounted on combine header. This was done using a spring-loaded four-bar linkage that would react with variations in the row and from driver error. A piece of flat metal stock was used to guide stalks to the sensor's face and had adequate length to prevent oscillations from occurring between stalks. The bracket had horizontal and vertical adjustment to position the sensor relative to the stalks. Care was taken in the bracket design to insure that the front wheel of the tractor did not bind with it when turning.

Laboratory Test

Water Standard

In July 2000, a laboratory test with two objectives was performed. The first objective was to gather information about the electric field generated by the sensor head. The second was to determine whether variation in excitation signal frequency or amplitude significantly affected electric field strength. The sensor was fixed, and a vile of water placed in front of the sensor head at many locations on a pre-defined grid. The grid, illustrated in figure 21, was comprised of three rows and six columns, which combine to yield 18 different locations. Row spacing was two inches, and column spacing was 0.5 inches. Four frequencies (100, 200, 300, and 400 kHz) and three voltages (0.25, 1.50, and 2.75 Volts peak-to-peak (V_{pp})) were measured at each location with a digital voltmeter on

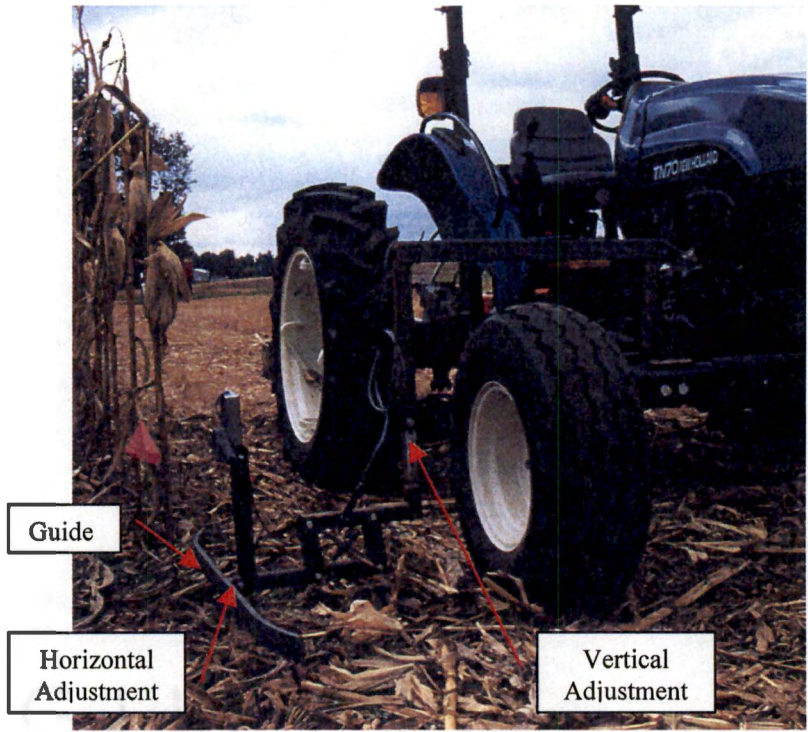


Figure 20. Tractor-mounting bracket used to accurately position sensor face a defined distance from the stalks at an operating height.

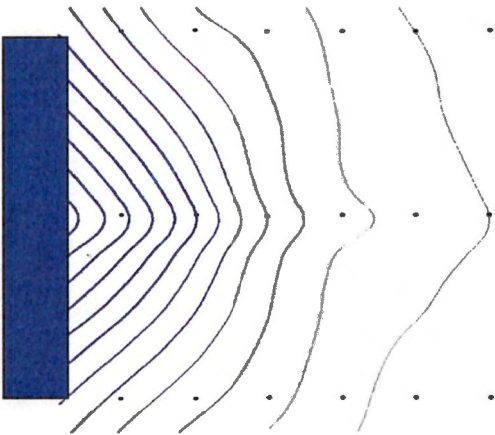


Figure 21. Test grid measurement locations and sensor field lines.

the bridge output.

Comparison Test

Further laboratory testing was performed in October 2000. This test was conducted to compare the prototype sensor and the commercial sensor specified by Nichols (2000), which was an Effector Inc. model KB5004. As seen in figure 22, both devices were mounted on the laboratory test stand, along with a light sensor (Micro Switch), which was used to provide the actual count. The commercial and light sensors were connected to a 21X Micrologger, which recorded their digital outputs. The prototype sensor was connected to its data acquisition system. A switch linked the two data

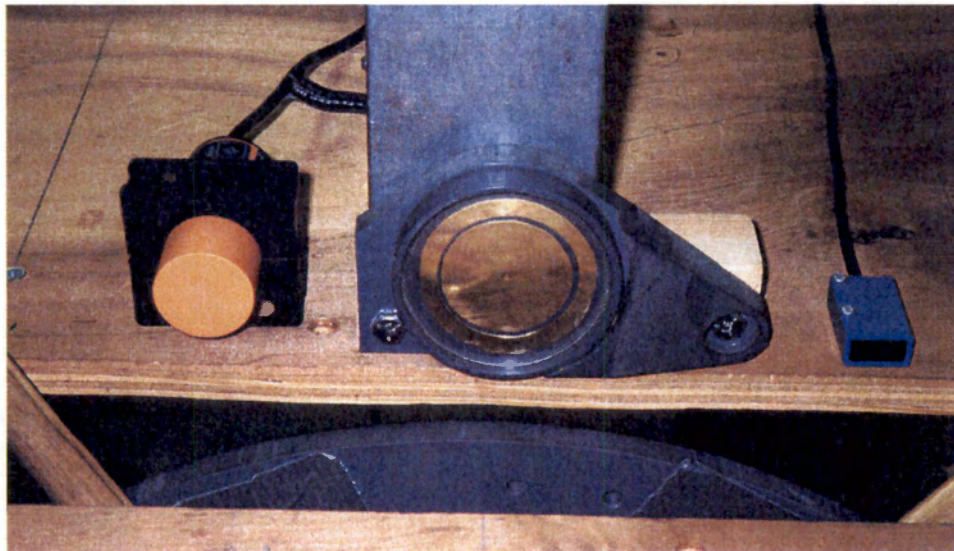


Figure 22. Mounting arrangement of prototype and commercial sensor on test stand.

acquisition systems so that data-collection would be synchronized for the three sensors. Actual corn stalks were mounted in the test stand wheel to compare the sensors. Tests consisted of two distances, three speeds, and two stalk-moisture contents. Five replications were performed for each combination. Stalk moisture contents of 0% and 40% wet basis (w.b.) were used along with distances of $\frac{3}{8}$ and $\frac{3}{4}$ inch, and speeds of 11.25, 30, and 44 RPM, which equates to combine ground speeds of 0.67, 1.78, and 2.62 mph, respectively. Measured stalk counts from the two sensors were compared to the actual count measured by the light sensor.

Field Test

The prototype sensor was tested on a New Holland TN70 tractor and a John Deere 4425 combine between October 16 and 19, 2000, at The University of Tennessee Milan Experiment Station in Milan, Tennessee. The sensor was first mounted to the tractor as previously described for controlled replicated tests. Tests were conducted at speeds of 0.40 and 1.76 mph on rows that had stalk counts of 10, 25, and 100 with an average spacing of 8 inches. Faster speeds than 1.76 mph were attempted; however, more stalks were being knocked over than counted so faster speed tests were abandoned. The 10 and 25 count rows had three replications and the 100-stalk row had six. Representative stalks were removed and packaged from these rows for later determination of their moisture content. The sensor was then mounted on the combine for final field-testing. Combine tests were conducted at 2 different ground speeds of 1.9 and 4.0 mph for rows of 10 stalks, and only 4.0 mph on rows of 100 stalks. No replications were made due to the

combine's destructive nature on the crop, so different rows were used each time. Six runs of 10-stalk rows and 3 runs of 100 stalks were completed. Weather conditions throughout the testing were warm and dry. Unfortunately many corn stalks were down due to a corn borer problem. Thus, fallen stalks were removed prior to testing.

Chapter 4--Results

Laboratory Evaluation

Water Standard

Results indicate that all 4 frequencies (100, 200, 300, and 400 kHz) significantly affected system output signal level ($P < 0.0001$; $\alpha = 0.05$). This corroborates Baxter (1997) stating that using higher frequencies provides higher signal-to-noise by reducing sensor impedance. Frequencies of 200 and 400 kHz were statistically different; however, 100 and 300 kHz were not statistically different than 200 and 400 kHz. Recall (Baxter, 1997) that a frequency of 400 kHz was used for the system because of an increase in sensitivity over the lower frequencies. Frequencies higher than 400 kHz presented problems due to the frequency limits of the circuitry.

All voltages (0.25, 1.50, and 2.75 V_{pp}) tested, significantly affected the output signal level ($P < 0.005$; $\alpha = 0.05$), and every voltage was statistically different. Tests results indicated that higher voltages provided greater sensing distance. The greatest sensing distance was obtained when using 2.75 V_{pp} . Greater sensing distances could be achieved with higher voltages, which create stronger electric fields; however, 2.75 V_{pp} was the maximum for the given circuitry design.

While using the 400 kHz and 2.75 V_{pp} to maximize system performance, the maximum sensing distance with a vile of water ($\epsilon_o = 1$) was 3 inches. Distances greater than 3 inches provided no valid output from the system due to low signal-to-noise values.

Signal-to-noise ratio at the bridge output for the vile of water at the sensor face was 1.05. The maximum sensing distance of a 40%(w.b.) moisture content stalk was determined to be 1.5 inches. This is in accordance with Baxter (1997) who states that sensing distance is based on the dielectric constant present. An illustration of the prototype sensor's electric field strength is seen in figure 23. Refer to figure 21 for illustration of sensor field lines and test grid.

Comparison Test

A second objective of the laboratory testing was to quantify performance of both the prototype sensor and the commercial capacitive proximity sensor in a side-by-side test. Recall that the prototype and commercial sensors were mounted to the test stand to determine performance at three speeds (0.67, 1.78, and 2.62 mph), two moisture contents (0% and 40%(w.b.)) and two stalk distances (3/8 and 3/4 inch) away from the sensor face.

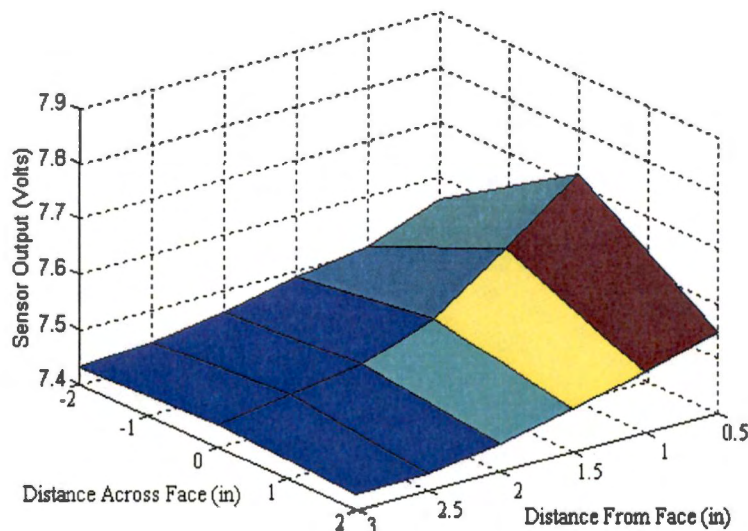


Figure 23. Prototype sensor's sensitivity resulting from electric field strength in the presence of water.

Comparison data were collected and percent error was determined using the following formula.

$$E = \frac{PS - AS}{AS} * 100 \quad \text{Equation VI}$$

where E = percent error

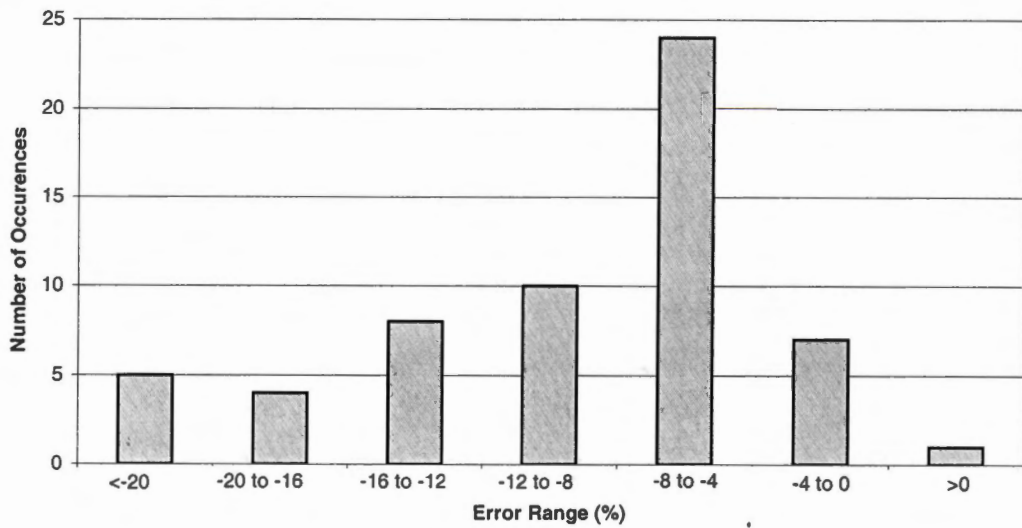
PS = predicted stalk count

AS = actual stalk count

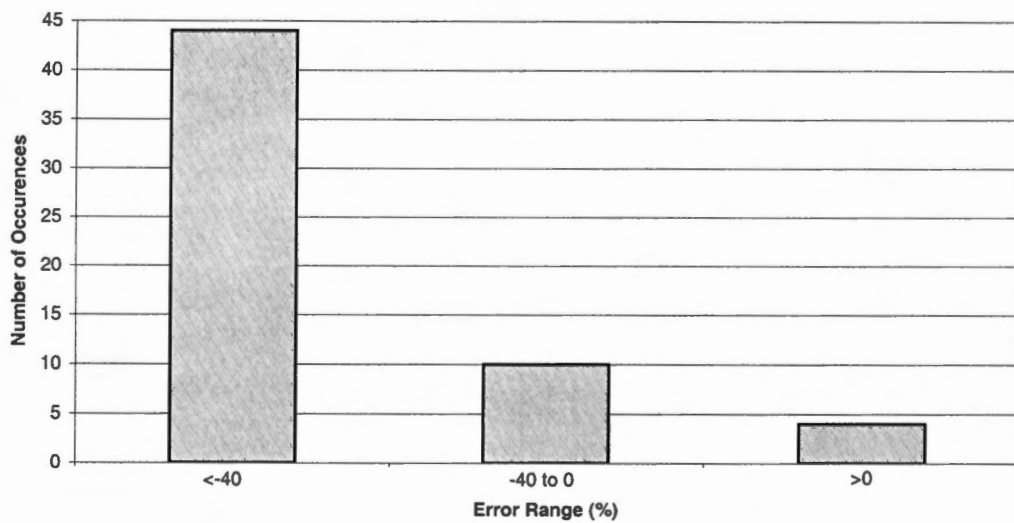
Distribution of error terms for the prototype and commercial sensors are shown in figure 24(a) and figure 24(b). Error distribution of the prototype suggest that the system under predicts 4 to 8 percent of the time. However, the commercial sensor under predicts greater then 40 percent of the time. Absolute value of average error terms for the prototype and commercial sensors are 5.6 percent and 78.0 percent respectively.

Distribution of error for different speeds, moisture contents, and distances are shown in table 1 for the prototype and commercial sensor.

Analysis of variance was used to determine if speed, distance or moisture content affected the prototype system's performance using the signed error and the absolute error of each sensor. All 3 variables proved to affect the systems overall performance ($P < 0.05$, $\alpha = 0.05$) for both error terms. Mean separation was used to determine if differences existed between the varying speeds, frequencies and distances. Mean separation indicated that no significant difference existed for the low and medium class speeds for the prototype sensor's absolute and signed error terms at the 95% confidence level; however,



(a)



(b)

Figure 24. Distribution of errors from the October, 2000 laboratory test. (a) The prototype sensor, and (b) the commercial sensor.

Table 1. Prototype and Commercial sensor error at different speeds, moisture contents, and distances.

Operating Parameters			Error (%)	
Speed(mph)	Moisture (%)	Distance(inch)	Prototype	Commercial
0.67	0	3/8	12.15	100.00
0.67	0	3/4	8.88	100.00
0.67	40	3/4	7.00	100.00
0.67	40	3/8	11.40	2.69
1.78	0	3/8	10.30	100.00
1.78	0	3/4	21.35	100.00
1.78	40	3/4	5.54	100.00
1.78	40	3/8	5.74	0.00
2.62	0	3/8	5.39	100.00
2.62	0	3/4	18.24	100.00
2.62	40	3/4	3.60	100.00
2.62	40	3/8	5.61	33.12

all others were significantly different. Analysis of variance was not performed on the commercial sensor due to limited number of times it actually worked (15 out of 60). All of these results were deemed adequate to justify that the prototype sensor overwhelmingly out-performed the commercial sensor.

Field Evaluation

The field test performed during the 2000 harvest season was designed to meet several objectives. The main objective was to determine if system accuracy obtained under controlled laboratory conditions could be repeated under normal field conditions. However, several factors were present that affect the system accuracy comparison between field and lab: plant spacing, harvester speed, and dynamic limitations of hardware and software.

Minimum plant spacing was determined to be 3 inches. If stalks were spaced closer than 3 inches along the row, there would be a stalk present in the sensing field at all times. For this reason, rows with stalks closer than 3 inches apart were removed. It was later determined with stalks taken and sealed at the time of testing that stalk moisture content was 20%(w.b.).

Tractor-Mounted Sensor Test

Testing was performed with the prototype mounted on the tractor bracket at two tractor ground speeds of 0.4 and 1.76 mph. Known stalk counts of 10, 25, and 100 were used with 3 replications being performed at 10 and 25 stalk counts. A total of 6 replications were performed on rows with 100 stalk counts. Data were collected and percent error determined. Average absolute error term for the system was 11.9 percent with a standard deviation of 8.3. Average absolute error terms were 8.9 percent and 16.0 percent for speeds of 0.4 mph and 1.76 mph, respectively. The error distribution of error terms can be seen in figure 25. The error distribution of the system was concentrated between -20 to -8 percent. A correlation coefficient of 0.43 ($P < 0.05$) relating speed and absolute percent error indicates a moderate relationship between the 2 variables. Both speeds were determined to be statistically significant to system performance ($P < 0.0001$; $\alpha = 0.05$) and the mean errors were statistically different.

Preliminary Combine-Mounted Sensor Test

After tractor-mounted sensor testing was complete the sensor was mounted on the combine as illustrated in figure 13, and runs of 10 and 100 stalks were performed at varying speeds (0.40 and 1.76 mph). Results from this test were inconclusive due to the

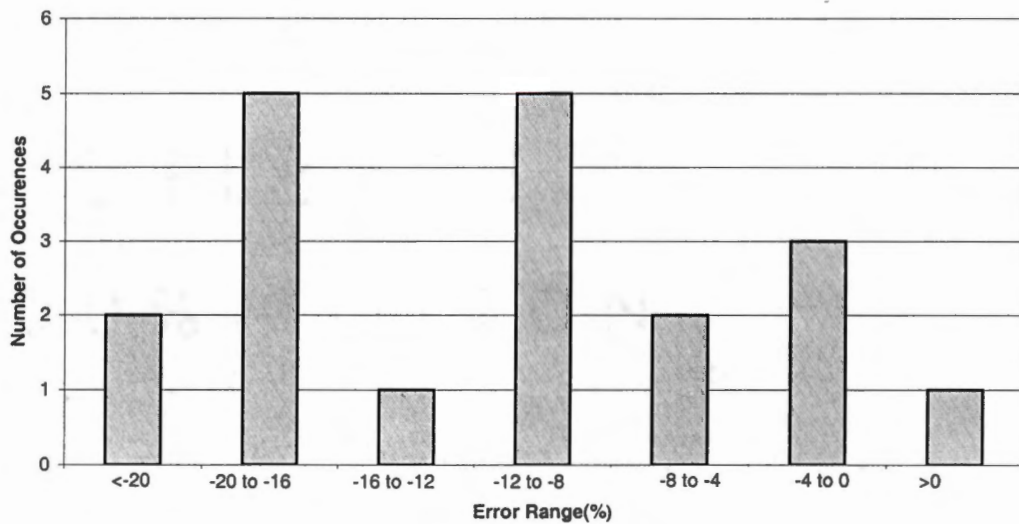


Figure 25. Distribution of errors from the October, 2000 tractor-mounted sensor test.

crop flowing past the sensor face at a spacing along the row so close it was almost as if it were a sheet. This was due to the stalks not being totally perpendicular to the ground. The stalks were severely leaning due to disease and late season harvest, and when the combine cowl started guiding them toward the snap rollers, they would drag along them and build-up forming the fore mentioned sheet. If stalks were in better condition valid results could be obtained because stalks would not be flowing past the sensor face like a sheet.

Dynamic Limitations

The main factor that could affect system performance is the dynamic limitations of the system. This was determined by analyzing the tractor data at simulated speeds. Speeds were accomplished by averaging data to simulate increasing and decreasing

tractor ground speeds. A moving average was passed through the data to reduce it and in effect doubling the speed. Expansion of the data was accomplished by taking the average of two data points and inserting this value in-between the two averaged values. The next two data points were selected and the process performed again until all the data were expanded effectively doubling the speed. Speeds of 0.2 and 4 mph were accomplished by this procedure. With the decreased speed, the software's average absolute percent error was 14.1 (Std. dev. 8.1) and average signed error was -6.9 (Std. dev. 15.0). The increase in speed produced average absolute percent error of 15.6 (Std. dev. 10.5) and average signed error of -14.1 (Std. dev. 12.6). Both of these tests provide proof that varying speeds did not affect the software's performance, since the average absolute percent error was 11.9 (Std. dev. 8.3) and average signed error was -11.7 (Std. dev. 8.6) for the original data.

Chapter 5--Conclusions and Recommendations

Conclusions

A system was designed for sensing of corn stalks flowing into a combine corn head. The system was prototyped, and after laboratory testing, was installed on a tractor mounting bracket and a John Deere 4425 combine during October, 2000 for field-testing. Field test results indicate that the system is capable of measuring corn stalk population. Tractor-mounted sensor test average absolute errors were 8.9 percent and 16.0 percent for speeds of 0.4 mph and 1.76 mph, respectively. However, the combine results were inconclusive due to downed stalks stemming from insect damage. With a few modifications, system accuracy could be greatly increased.

Recommendations

System Refinements

Several refinements are necessary to increase system accuracy and reduce system size. Better methods for zeroing the bridge need to be investigated in order to increase sensitivity. Sensor size needs to be investigated to evaluate the trade-off between sensing distance and plant spacing. A reduction in sensor face size will reduce overall sensing distance but will reduce the problem of close stalk sensing. Circuitry can be reduced in size so that it will mount easily in the back of the mounting bracket. Signal processing software can be replaced with the circuitry shown in figure 26. This circuitry is designed with operational amplifiers and assorted passive components. Circuitry will allow continuous operation because data storage will no longer be an issue since only a count

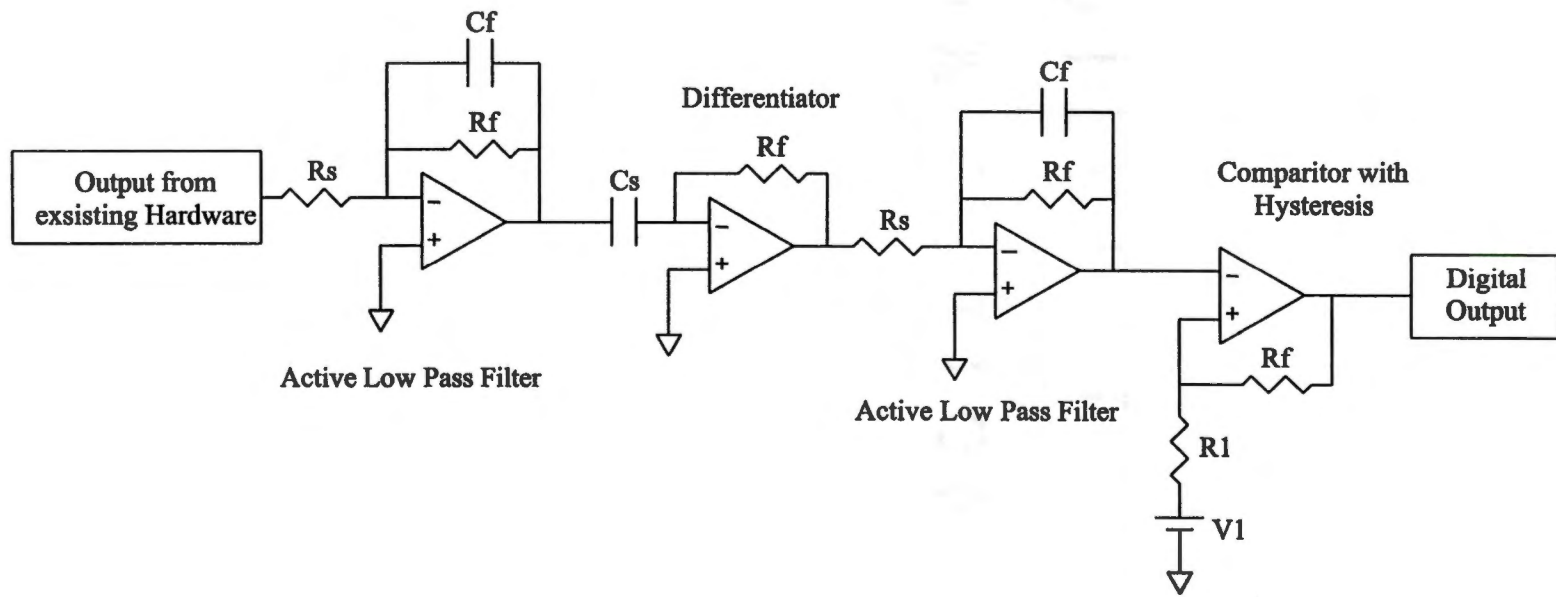


Figure 26. Circuit schematic of processing circuit to replace software.

will be recorded. It will reduce system complexity by eliminating the computer and data acquisition components.

Additional Testing

Future testing should be broadened to include investigation of several factors. Testing on high weed density rows would provide insight into whether the sensor can distinguish between weeds and stalks. Corn needs to be harvested throughout the harvest season to insure that broad ranges of moisture contents are evaluated. The system also needs to be run at multiple harvesting speeds. Additional testing which includes all of these factors is critical to insure that the system produces adequate results.

GILBERT

100% COTTON

References

- Barbosa, R. N. 1996. Site-specific applications of nitrogen in corn based on yield potential. M.S. thesis. The University of Tennessee.
- Baxter, L. K. 1997. *Capacitive Sensors Design and Applications*. New York: IEEE Press.
- Birrell, S., K.A. Sudduth. 1995. Corn population for precision farming. In *Proc. ASAE Annual Meeting*. Chicago, Illinois., 18-23 June.
- Chan et al. 1996. Solid-state micro proximity sensor. US Patent No. 5512836.
- Dally, J. W., W. F. Riley, K. G. McConnell. 1993. *Instrumentation for Engineering Measurements* 2nd edition. New York: John Wiley & Sons, Inc.
- Doerge, T. 1999. New opportunities in variable-rate seeding of corn. Pioneer Seed Company. Des Moines, IA.
- Han, S., S. M. Schneider, S. L. Rawlins and R. G. Evans. 1997. A bitmap method for determining effective combine cut width in yield mapping. *Transactions of the ASAE* 40(2): 485-490.
- Harrington, J. 2000. Understand cause of low yields before varying seeding rates. Pioneer Seed Company. Des Moines, IA.
- Hillyer, G., D. Miller. 1998. Getting started with precision farming. *Progressive Farmer Magazine*. March.
- Matsch, L. W. 1964. *Capacitors, Magnetic Circuits, and Transformers*. N.J.: Prentice-Hall, Inc.
- Moody, F. H. 1998. Development and Evaluation of a real-time cotton flow rate sensor. M.S. thesis. The University of Tennessee.
- MSI. 1998. Operating Properties for a Typical Piezo Film Element. Measurement Specialties Incorporated. Valley Forge, PA.
- Nichols, S. W. 2000. Method and apparatus for counting crops. US Patent No. 6073427.
- Norman, C. L. 2000. Field crops seeding guide. University of Tennessee Extension Service. Knoxville, TN.
- Patrico, J. 1999. Get the most from your yield monitor. *Progressive Farmer Magazine*. September.

Reitz, P., H. D. Kutzbach. 1996. Investigations on a particular yield mapping system for combine harvesters. *Computers and Electronics in Agriculture* 14(September): 137-150.

Rizzoni, G. 1996. *Principles and applications of electrical engineering*. IL: Times Mirror Higher Education Group Inc.

Stafford, J.V., B. Ambler and H. C. Bolam. 1997. Cut width sensors to improve the accuracy of yield mapping systems. In *Proc. European Conference on Precision Agriculture*, 519-527. Warwick University, UK., September.

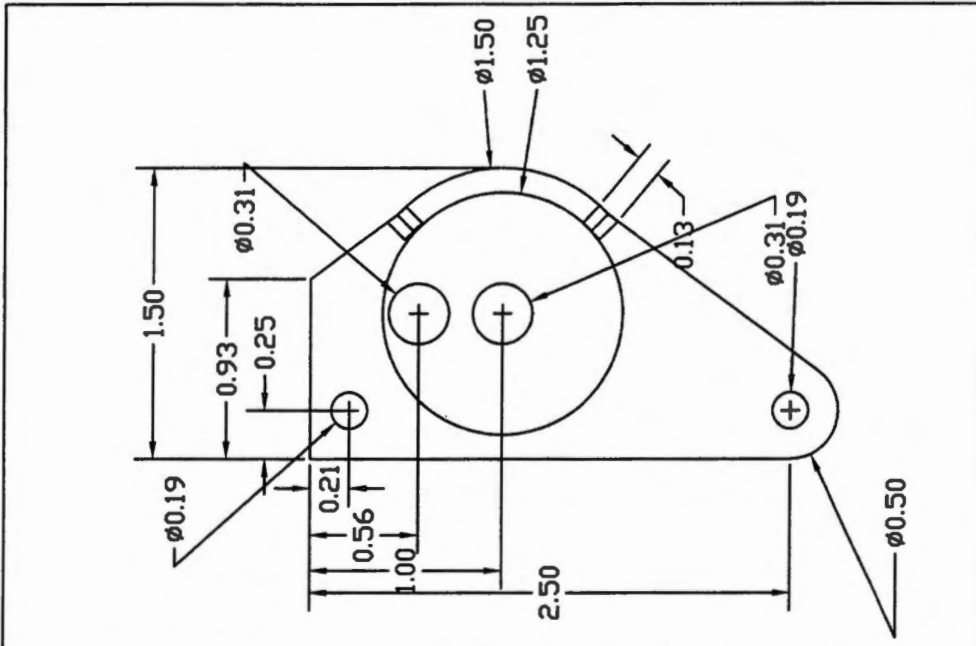
Warring, R. H., S. Gibilisco. 1985. *Fundamentals of Transducers*. PA: Tab Books Inc.

GILBERT
100% COTTON

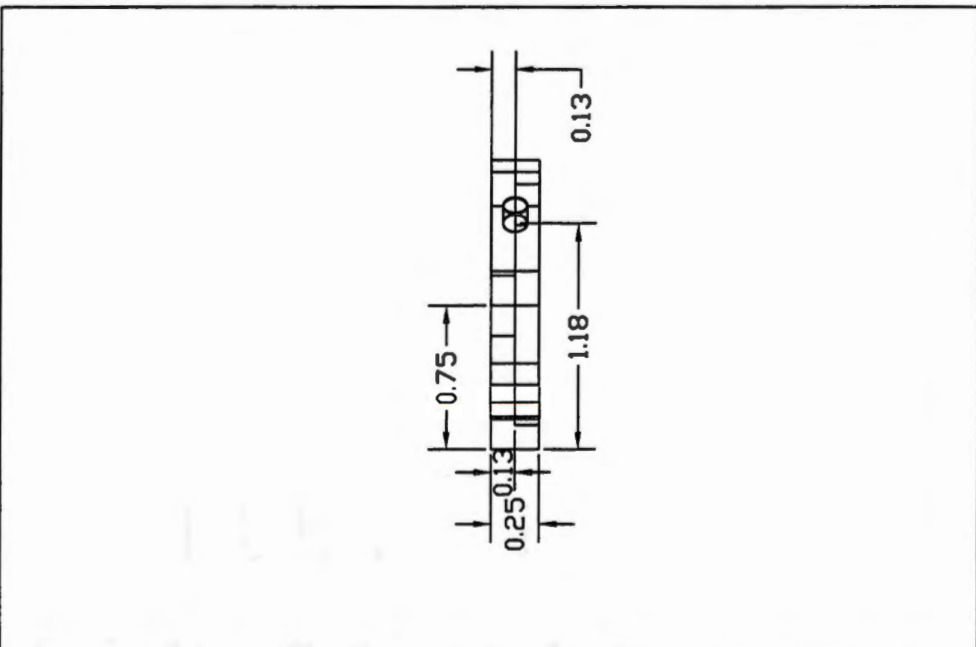
Appendices

CONFIDENTIAL
100% CONFIDENTIAL

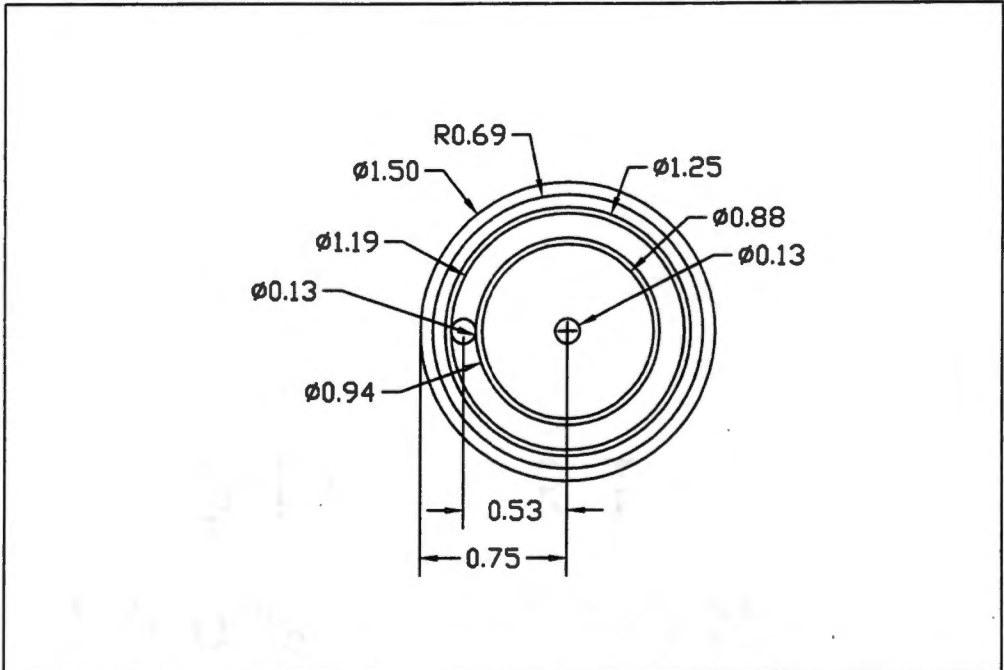
Appendix A
Mechanical Drawings



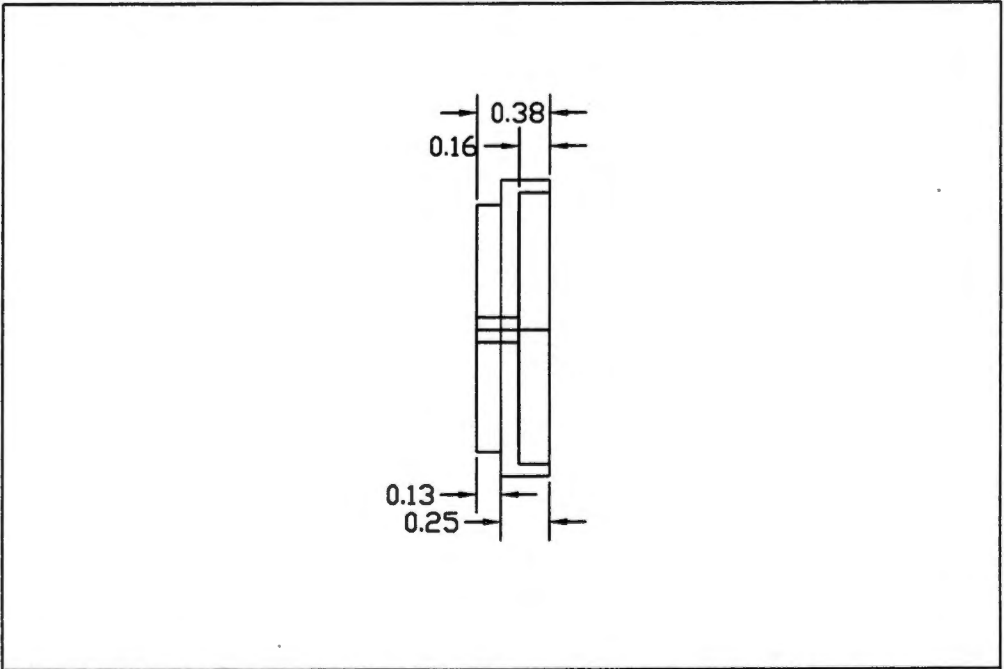
UT. Ag. Eng. Dept.	Title: Bracket	Drawing: 1	Scale: 1/2
Project: Voo-doo	Date: 9/10/00	Sheet: 1	Newman Webb



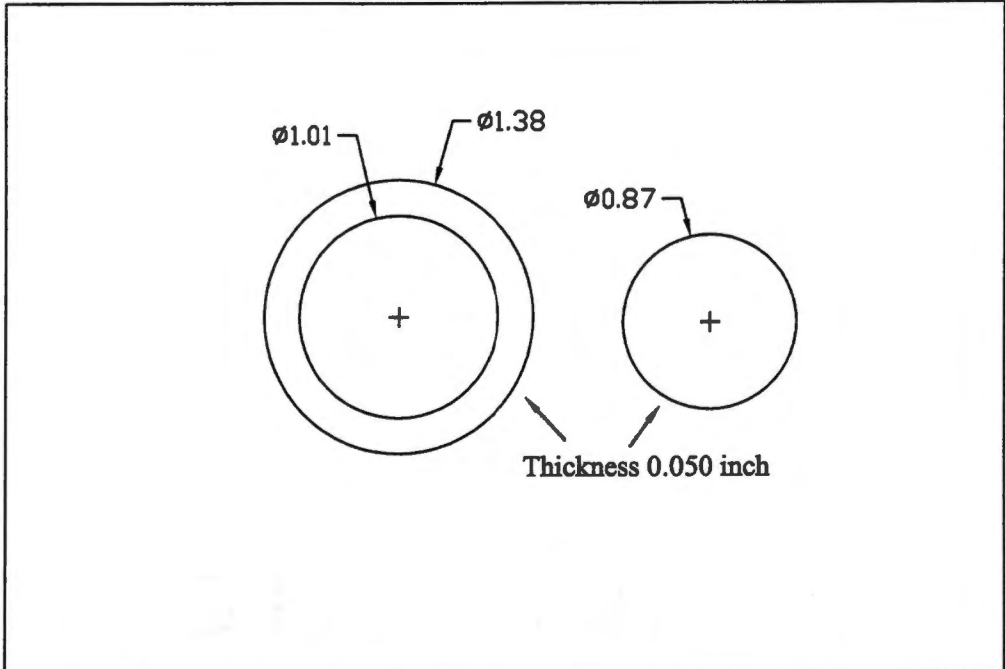
UT. Ag. Eng. Dept.	Title: Bracket	Drawing: 2	Scale: 1/2
Project: Voo-doo	Date: 9/10/00	Sheet: 1	Newman Webb



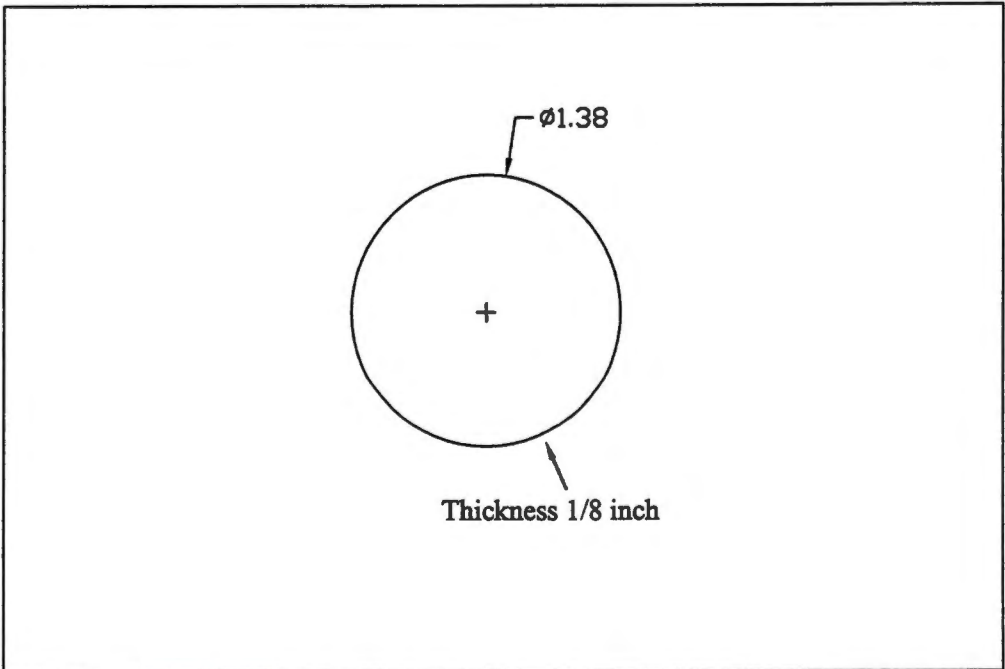
UT. Ag. Eng. Dept.	Title: Head	Drawing: 3	Scale: 1/2
Project: Voo-doo	Date: 9/10/00	Sheet: 1	Newman Webb



UT. Ag. Eng. Dept.	Title: Head	Drawing: 3	Scale: 1/2
Project: Voo-doo	Date: 9/10/00	Sheet: 2	Newman Webb



UT. Ag. Eng. Dept.	Title: Disc and Ring	Drawing: 4	Scale: 1/2
Project: Voo-doo	Date: 9/10/00	Sheet: 1	Newman Webb



UT. Ag. Eng. Dept.	Title: Lexan Cover	Drawing: 4	Scale: 1/2
Project: Voo-doo	Date: 9/10/00	Sheet: 1	Newman Webb

0113-21
100% DESIGN

Appendix B
Electronic Device Specifications

LM7171

Very High Speed, High Output Current, Voltage Feedback Amplifier

General Description

The LM7171 is a high speed voltage feedback amplifier that has the slewing characteristic of a current feedback amplifier; yet it can be used in all traditional voltage feedback amplifier configurations. The LM7171 is stable for gains as low as +2 or -1. It provides a very high slew rate at 4100V/ μ s and a wide unity-gain bandwidth of 200 MHz while consuming only 6.5 mA of supply current. It is ideal for video and high speed signal processing applications such as HDSL and pulse amplifiers. With 100 mA output current, the LM7171 can be used for video distribution, as a transformer driver or as a laser diode driver.

Operation on $\pm 15V$ power supplies allows for large signal swings and provides greater dynamic range and signal-to-noise ratio. The LM7171 offers low SFDR and THD, ideal for ADC/DAC systems. In addition, the LM7171 is specified for $\pm 5V$ operation for portable applications.

The LM7171 is built on National's advanced VIP™ III (Vertically integrated PNP) complementary bipolar process.

- Easy-To-Use Voltage Feedback Topology
- Very High Slew Rate: 4100V/ μ s
- Wide Unity-Gain Bandwidth: 200 MHz
- -3 dB Frequency @ $A_v = +2$: 220 MHz
- Low Supply Current: 6.5 mA
- High Open Loop Gain: 85 dB
- High Output Current: 100 mA
- Differential Gain and Phase: 0.01%, 0.02°
- Specified for $\pm 15V$ and $\pm 5V$ Operation

Applications

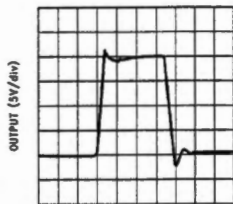
- HDSL and ADSL Drivers
- Multimedia Broadcast Systems
- Professional Video Cameras
- Video Amplifiers
- Copiers/Scanners/Fax
- HDTV Amplifiers
- Pulse Amplifiers and Peak Detectors
- CATV/Fiber Optics Signal Processing

Features

(Typical Unless Otherwise Noted)

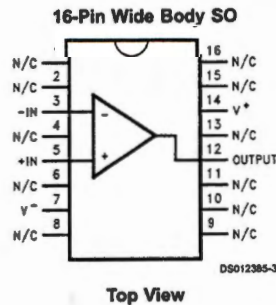
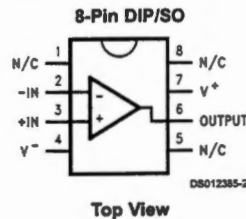
Typical Performance

Large Signal Pulse Response
 $A_v = +2, V_s = \pm 15V$



DS012385-1

Connection Diagrams



VIP™ is a trademark of National Semiconductor Corporation.

Absolute Maximum Ratings (Note 1)		Maximum Junction Temperature (Note 4)					
If Military/Aerospace specified devices are required, please contact the National Semiconductor Sales Office/Distributors for availability and specifications.		150°C					
ESD Tolerance (Note 2)		2.5 kV					
Supply Voltage (V ⁺ -V ⁻)		36V					
Differential Input Voltage (Note 11)		±10V					
Output Short Circuit to Ground (Note 3)		Continuous					
Storage Temperature Range		-65°C to +150°C					
Operating Ratings (Note 1)		Supply Voltage					
		5.5V ≤ V _S ≤ 36V					
Operating Ratings (Note 1)		Junction Temperature Range					
		-40°C ≤ T _J ≤ +85°C					
		LM7171AI, LM7171BI					
		Thermal Resistance (θ _{J-A})					
		N Package, 8-Pin Molded DIP 108°C/W					
		M Package, 8-Pin Surface Mount 172°C/W					
		M Package, 16-Pin Surface Mount 95°C/W					
±15V DC Electrical Characteristics							
Unless otherwise specified, all limits guaranteed for T _J = 25°C, V ⁺ = +15V, V ⁻ = -15V, V _{CM} = 0V, and R _L = 1 kΩ. Boldface limits apply at the temperature extremes							
Symbol	Parameter	Conditions	Typ (Note 5)	LM7171AI Limit (Note 6)	LM7171BI Limit (Note 6)	Units	
V _{os}	Input Offset Voltage		0.2	1	3	mV	
				4	7	max	
TC V _{os}	Input Offset Voltage Average Drift		35			μV/°C	
I _B	Input Bias Current		2.7	10	10	μA	
				12	12	max	
I _{os}	Input Offset Current		0.1	4	4	μA	
				6	6	max	
R _{in}	Input Resistance	Common Mode	40			MΩ	
		Differential Mode	3.3				
R _O	Open Loop Output Resistance		15			Ω	
CMRR	Common Mode Rejection Ratio	V _{CM} = ±10V	105	85	75	dB	
				80	70	min	
PSRR	Power Supply Rejection Ratio	V _S = ±15V to ±5V	90	85	75	dB	
				80	70	min	
V _{CM}	Input Common-Mode Voltage Range	CMRR > 60 dB	±13.35			V	
A _v	Large Signal Voltage Gain (Note 7)	R _L = 1 kΩ	85	80	75	dB	
				75	70	min	
		R _L = 100Ω	81	75	70	dB	
				70	66	min	
V _O	Output Swing	R _L = 1 kΩ	13.3	13	13	V	
					12.7	12.7	min
					-13	-13	V
				-12.7	-12.7	max	
		R _L = 100Ω	11.8	10.5	10.5	V	
					9.5	9.5	min
			-9.5	-9.5	V		
				-9	max		
Output Current (Open Loop) (Note 8)	Sourcing, R _L = 100Ω		118	105	105	mA	
				95	95	min	
	Sinking, R _L = 100Ω		105	95	95	mA	
				90	90	max	

±15V DC Electrical Characteristics (Continued)

Unless otherwise specified, all limits guaranteed for $T_J = 25^\circ\text{C}$, $V^+ = +15\text{V}$, $V^- = -15\text{V}$, $V_{\text{CM}} = 0\text{V}$, and $R_L = 1\text{ k}\Omega$. Boldface limits apply at the temperature extremes

Symbol	Parameter	Conditions	Typ (Note 5)	LM7171AI Limit (Note 6)	LM7171BI Limit (Note 6)	Units
	Output Current (in Linear Region)	Sourcing, $R_L = 100\Omega$	100			mA
		Sinking, $R_L = 100\Omega$	100			
I_{SC}	Output Short Circuit Current	Sourcing	140			mA
		Sinking	135			
I_S	Supply Current		6.5	8.5	8.5	mA
				9.5	9.5	

±15V AC Electrical Characteristics

Unless otherwise specified, $T_J = 25^\circ\text{C}$, $V^+ = +15\text{V}$, $V^- = -15\text{V}$, $V_{\text{CM}} = 0\text{V}$, and $R_L = 1\text{ k}\Omega$.

Symbol	Parameter	Conditions	Typ (Note 5)	LM7171AI Limit (Note 6)	LM7171BI Limit (Note 6)	Units
SR	Slew Rate (Note 9)	$A_V = +2$, $V_{\text{IN}} = 13\text{ V}_{\text{PP}}$	4100			V/ μs
		$A_V = +2$, $V_{\text{IN}} = 10\text{ V}_{\text{PP}}$	3100			
	Unity-Gain Bandwidth		200			MHz
	-3 dB Frequency	$A_V = +2$	220			MHz
ϕ_m	Phase Margin		50			Deg
t_s	Settling Time (0.1%)	$A_V = -1$, $V_O = \pm 5\text{V}$ $R_L = 500\Omega$	42			ns
t_p	Propagation Delay	$A_V = -2$, $V_{\text{IN}} = \pm 5\text{V}$, $R_L = 500\Omega$	5			ns
A_D	Differential Gain (Note 10)		0.01			%
ϕ_D	Differential Phase (Note 10)		0.02			Deg
		Second Harmonic (Note 12)				
		$f_{\text{IN}} = 10\text{ kHz}$	-110			dBc
		$f_{\text{IN}} = 5\text{ MHz}$	-75			dBc
	Third Harmonic (Note 12)	$f_{\text{IN}} = 10\text{ kHz}$	-115			dBc
		$f_{\text{IN}} = 5\text{ MHz}$	-55			dBc
e_n	Input-Referred Voltage Noise	$f = 10\text{ kHz}$	14			$\frac{\text{nV}}{\sqrt{\text{Hz}}}$
i_n	Input-Referred Current Noise	$f = 10\text{ kHz}$	1.5			$\frac{\text{pA}}{\sqrt{\text{Hz}}}$

±5V DC Electrical Characteristics

Unless otherwise specified, all limits guaranteed for $T_J = 25^\circ\text{C}$, $V^+ = +5\text{V}$, $V^- = -5\text{V}$, $V_{\text{CM}} = 0\text{V}$, and $R_L = 1\text{ k}\Omega$. Boldface limits apply at the temperature extremes

Symbol	Parameter	Conditions	Typ (Note 5)	LM7171AI Limit (Note 6)	LM7171BI Limit (Note 6)	Units
V_{OS}	Input Offset Voltage		0.3	1.5	3.5	mV
TC V_{OS}	Input Offset Voltage Average Drift		35	4	7	$\mu\text{V}/^\circ\text{C}$
I_B	Input Bias Current		3.3	10	10	μA
				12	12	
I_{OS}	Input Offset Current		0.1	4	4	μA

LM7171 Circuit Operation (Continued)

ers the inverting input. The triple-buffered output stage isolates the gain stage from the load to provide low output impedance.

LM7171 Slew Rate Characteristic

The slew rate of LM7171 is determined by the current available to charge and discharge an internal high impedance node capacitor. This current is the differential input voltage divided by the total degeneration resistor R_E . Therefore, the slew rate is proportional to the input voltage level, and the higher slew rates are achievable in the lower gain configurations. A curve of slew rate versus input voltage level is provided in the "Typical Performance Characteristics".

When a very fast large signal pulse is applied to the input of an amplifier, some overshoot or undershoot occurs. By placing an external resistor such as 1 k Ω in series with the input of LM7171, the bandwidth is reduced to help lower the overshoot.

Slew Rate Limitation

If the amplifier's input signal has too large of an amplitude at too high of a frequency, the amplifier is said to be slew rate limited; this can cause ringing in time domain and peaking in frequency domain at the output of the amplifier.

In the "Typical Performance Characteristics" section, there are several curves of $A_{Vf} = +2$ and $A_{Vf} = +4$ versus input signal levels. For the $A_{Vf} = +4$ curves, no peaking is present and the LM7171 responds identically to the different input signal levels of 30 mV, 100 mV and 300 mV.

For the $A_{Vf} = +2$ curves, with slight peaking occurs. This peaking at high frequency (>100 MHz) is caused by a large input signal at high enough frequency that exceeds the amplifier's slew rate. The peaking in frequency response does not limit the pulse response in time domain, and the LM7171 is stable with noise gain of ≥ 2 .

Layout Consideration

PRINTED CIRCUIT BOARDS AND HIGH SPEED OP AMPS

There are many things to consider when designing PC boards for high speed op amps. Without proper caution, it is very easy to have excessive ringing, oscillation and other degraded AC performance in high speed circuits. As a rule, the signal traces should be short and wide to provide low inductance and low impedance paths. Any unused board space needs to be grounded to reduce stray signal pickup. Critical components should also be grounded at a common point to eliminate voltage drop. Sockets add capacitance to the board and can affect high frequency performance. It is better to solder the amplifier directly into the PC board without using any socket.

USING PROBES

Active (FET) probes are ideal for taking high frequency measurements because they have wide bandwidth, high input impedance and low input capacitance. However, the probe ground leads provide a long ground loop that will produce errors in measurement. Instead, the probes can be grounded directly by removing the ground leads and probe jacks and using scope probe jacks.

COMPONENT SELECTION AND FEEDBACK RESISTOR

It is important in high speed applications to keep all component leads short. For discrete components, choose carbon composition-type resistors and mica-type capacitors. Surface mount components are preferred over discrete components for minimum inductive effect.

Large values of feedback resistors can couple with parasitic capacitance and cause undesirable effects such as ringing or oscillation in high speed amplifiers. For LM7171, a feedback resistor of 510 Ω gives optimal performance.

Compensation for Input Capacitance

The combination of an amplifier's input capacitance with the gain setting resistors adds a pole that can cause peaking or oscillation. To solve this problem, a feedback capacitor with a value

$$C_F > (R_G \times C_{in})/R_F$$

can be used to cancel that pole. For LM7171, a feedback capacitor of 2 pF is recommended. Figure 1 illustrates the compensation circuit.

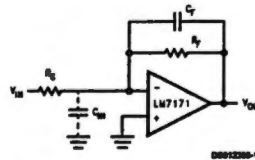


FIGURE 1. Compensating for Input Capacitance

Power Supply Bypassing

Bypassing the power supply is necessary to maintain low power supply impedance across frequency. Both positive and negative power supplies should be bypassed individually by placing 0.01 μ F ceramic capacitors directly to power supply pins and 2.2 μ F tantalum capacitors close to the power supply pins.

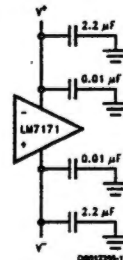


FIGURE 2. Power Supply Bypassing

Termination

In high frequency applications, reflections occur if signals are not properly terminated. Figure 3 shows a properly terminated signal while Figure 4 shows an improperly terminated signal.

Termination (Continued)

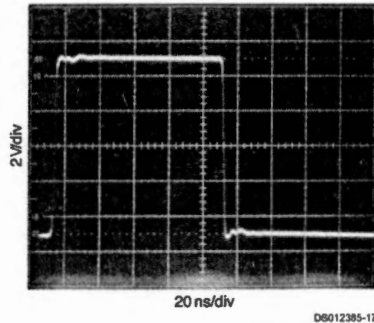


FIGURE 3. Properly Terminated Signal

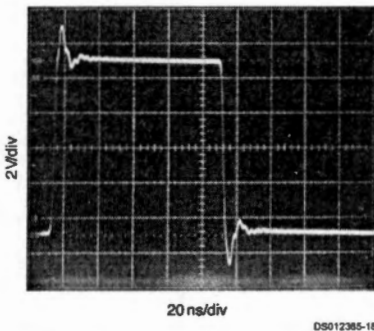


FIGURE 4. Improperly Terminated Signal

To minimize reflection, coaxial cable with matching characteristic impedance to the signal source should be used. The other end of the cable should be terminated with the same value terminator or resistor. For the commonly used cables, RG59 has 75Ω characteristic impedance, and RG58 has 50Ω characteristic impedance.

Driving Capacitive Loads

Amplifiers driving capacitive loads can oscillate or have ringing at the output. To eliminate oscillation or reduce ringing, an isolation resistor can be placed as shown below in Figure 5. The combination of the isolation resistor and the load capacitor forms a pole to increase stability by adding more phase margin to the overall system. The desired performance depends on the value of the isolation resistor; the bigger the isolation resistor, the more damped the pulse response becomes. For LM7171, a 50Ω isolation resistor is recommended for initial evaluation. Figure 6 shows the LM7171 driving a 150 pF load with the 50Ω isolation resistor.

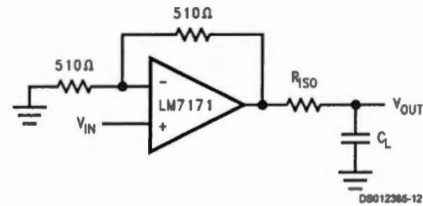


FIGURE 5. Isolation Resistor Used to Drive Capacitive Load

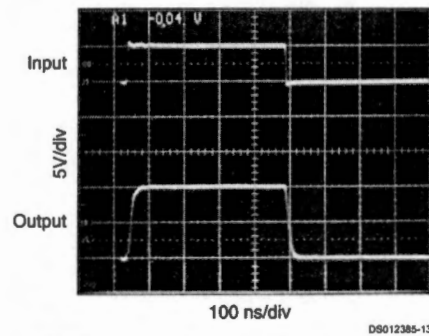


FIGURE 6. The LM7171 Driving a 150 pF Load with a 50Ω Isolation Resistor

Power Dissipation

The maximum power allowed to dissipate in a device is defined as:

$$P_D = (T_{J(max)} - T_A) / \theta_{JA}$$

Where

- P_D is the power dissipation in a device
- $T_{J(max)}$ is the maximum junction temperature
- T_A is the ambient temperature
- θ_{JA} is the thermal resistance of a particular package

For example, for the LM7171 in a SO-8 package, the maximum power dissipation at 25°C ambient temperature is 730 mW.

Thermal resistance, θ_{JA} , depends on parameters such as die size, package size and package material. The smaller the die size and package, the higher θ_{JA} becomes. The 8-pin DIP package has a lower thermal resistance (108°C/W) than that of 8-pin SO (172°C/W). Therefore, for higher dissipation capability, use an 8-pin DIP package.

The total power dissipated in a device can be calculated as:

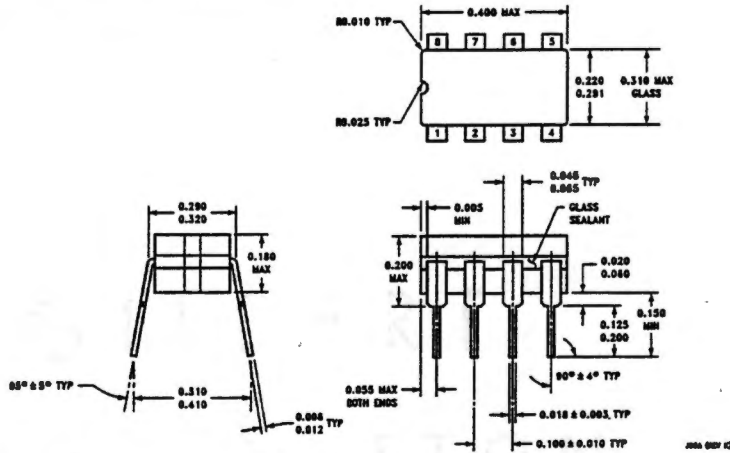
$$P_D = P_Q + P_L$$

P_Q is the quiescent power dissipated in a device with no load connected at the output. P_L is the power dissipated in the device with a load connected at the output; it is not the power dissipated by the load.

Furthermore,

- P_Q : = supply current x total supply voltage with no load
- P_L : = output current x (voltage difference between supply voltage and output voltage of the same side of supply voltage)

Physical Dimensions inches (millimeters) unless otherwise noted (Continued)



Order Number 5962-8553801QPA
 8-Lead Dual-in-Line Package
 NS Package Number J08A
 NSID is LM7171AMJ883

LIFE SUPPORT POLICY

NATIONAL'S PRODUCTS ARE NOT AUTHORIZED FOR USE AS CRITICAL COMPONENTS IN LIFE SUPPORT DEVICES OR SYSTEMS WITHOUT THE EXPRESS WRITTEN APPROVAL OF THE PRESIDENT AND GENERAL COUNSEL OF NATIONAL SEMICONDUCTOR CORPORATION. As used herein:

1. Life support devices or systems are devices or systems which, (a) are intended for surgical implant into the body, or (b) support or sustain life, and whose failure to perform when properly used in accordance with instructions for use provided in the labeling, can be reasonably expected to result in a significant injury to the user.
2. A critical component is any component of a life support device or system whose failure to perform can be reasonably expected to cause the failure of the life support device or system, or to affect its safety or effectiveness.

 <p>National Semiconductor Corporation Americas Tel: 1-800-272-0988 Fax: 1-800-737-7018 Email: support@nsc.com www.national.com</p>	<p>National Semiconductor Europe Fax: +49 (0) 1 80-630 85 88 Email: europe.support@nsc.com Deutsch Tel: +49 (0) 1 80-630 85 85 English Tel: +49 (0) 1 80-632 78 32 Francaise Tel: +49 (0) 1 80-632 83 88 Italiana Tel: +49 (0) 1 80-634 18 88</p>	<p>National Semiconductor Asia Pacific Customer Response Group Tel: 65-2504468 Fax: 65-2504468 Email: asa.support@nsc.com</p>	<p>National Semiconductor Japan Ltd. Tel: 81-3-6638-7560 Fax: 81-3-6638-7507</p>
---	---	--	--

National does not assume any responsibility for use of any circuitry described, no circuit patent licenses are implied and National reserves the right at any time without notice to change said circuitry and specifications.

LM340/LM78MXX Series 3-Terminal Positive Regulators

General Description

The LM140/LM340A/LM340/LM7800C monolithic 3-terminal positive voltage regulators employ internal current-limiting, thermal shutdown and safe-area compensation, making them essentially indestructible. If adequate heat sinking is provided, they can deliver over 1.0A output current. They are intended as fixed voltage regulators in a wide range of applications including local (on-card) regulation for elimination of noise and distribution problems associated with single-point regulation. In addition to use as fixed voltage regulators, these devices can be used with external components to obtain adjustable output voltages and currents.

Considerable effort was expended to make the entire series of regulators easy to use and minimize the number of external components. It is not necessary to bypass the output, although this does improve transient response. Input bypassing is needed only if the regulator is located far from the filter capacitor of the power supply.

The 5V, 12V, and 15V regulator options are available in the steel TO-3 power package. The LM340A/LM340/LM7800C series is available in the TO-220 plastic power package, and the LM340-5.0 is available in the SOT-223 package, as well as the LM340-5.0 and LM340-12 in the surface-mount TO-263 package.

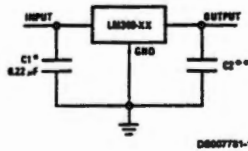
Features

- Complete specifications at 1A load
- Output voltage tolerances of $\pm 2\%$ at $T_j = 25^\circ\text{C}$ and $\pm 4\%$ over the temperature range (LM340A)
- Line regulation of 0.01% of V_{OUT}/V of ΔV_{IN} at 1A load (LM340A)
- Load regulation of 0.3% of V_{OUT}/A (LM340A)
- Internal thermal overload protection
- Internal short-circuit current limit
- Output transistor safe area protection
- P* Product Enhancement tested

Device	Output Voltages	Packages
LM140	5, 12, 15	TO-3 (K)
LM340A/LM340	5, 12, 15	TO-3 (K), TO-220 (T), SOT-223 (MP), TO-263 (S) (5V and 12V only)
LM7800C	5, 8, 12, 15	TO-220 (T)

Typical Applications

Fixed Output Regulator

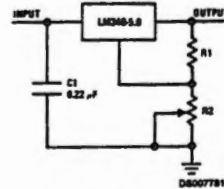


DS007781-1

*Required if the regulator is located far from the power supply filter.

**Although no output capacitor is needed for stability, it does help transient response. (If needed, use 0.1 µF, ceramic disc).

Adjustable Output Regulator

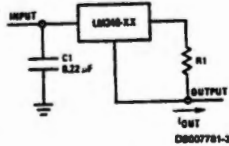


DS007781-2

$$V_{OUT} = 5V + (5V/R1 + I_Q) R2 \quad 5V/R1 > 3 I_Q$$

load regulation (L_L) = $[(R1 + R2)/R1] (L_L \text{ of LM340-5})$.

Current Regulator



DS007781-3

$$I_{OUT} = \frac{V2-3}{R1} + I_Q$$

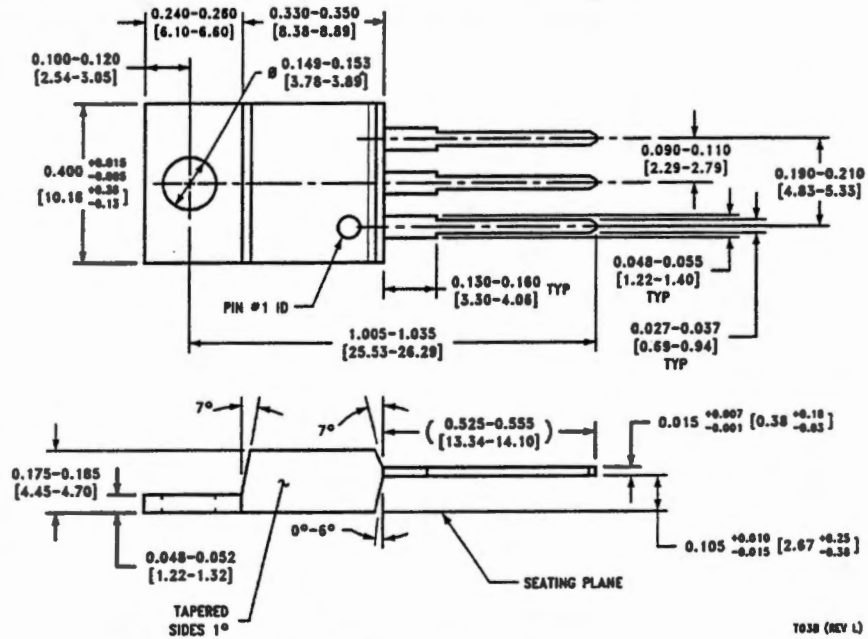
$\Delta I_Q = 1.3 \text{ mA}$ over line and load changes.

Comparison between SOT-223 and D-Pak (TO-252) Packages



Scale 1:1

Physical Dimensions inches (millimeters) unless otherwise noted (Continued)



T03B (REV L)

TO-220 Power Package (T)
Order Number LM340AT/LM340T-5.0, LM340AT/LM340T-12, LM340AT/LM340T-15,
LM7805CT, LM7812CT, LM7815CT, LM7806CT, LM7808CT, LM7818CT or LM7824CT
NS Package Number T03B

FEATURES

- Single Supply Operation
- Output Swings Rail to Rail
- Input Voltage Range Extends Below Ground
- Single Supply Capability from +3 V to +36 V
- High Load Drive
- Capacitive Load Drive of 500 pF, $G = +1$
- Output Current of 15 mA, 0.5 V from Supplies
- Excellent AC Performance on 2.6 mA/Amplifier
- 3 dB Bandwidth of 16 MHz, $G = +1$
- 350 ns Settling Time to 0.01% (2 V Step)
- Slew Rate of 22 V/ μ s
- Good DC Performance
- 800 μ V Max Input Offset Voltage
- 2 μ V/ $^{\circ}$ C Offset Voltage Drift
- 25 pA Max Input Bias Current
- Low Distortion
- 108 dBc Worst Harmonic @ 20 kHz
- Low Noise
- 16 nV/ $\sqrt{\text{Hz}}$ @ 10 kHz
- No Phase Inversion with Inputs to the Supply Rails

APPLICATIONS

- Battery Powered Precision Instrumentation
- Photodiode Preamps
- Active Filters
- 12- to 16-Bit Data Acquisition Systems
- Medical Instrumentation

PRODUCT DESCRIPTION

The AD823 is a dual precision, 16 MHz, JFET input op amp that can operate from a single supply of +3.0 V to +36 V, or dual supplies of ± 1.5 V to ± 18 V. It has true single supply capability with an input voltage range extending below ground in single supply mode. Output voltage swing extends to within 50 mV of each rail for $I_{OUT} \leq 100 \mu\text{A}$ providing outstanding output dynamic range.

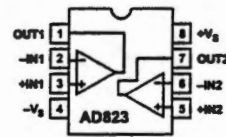
Offset voltage of 800 μV max, offset voltage drift of 2 $\mu\text{V}/^{\circ}\text{C}$, input bias currents below 25 pA and low input voltage noise provide dc precision with source impedances up to a Gigohm. 16 MHz, -3 dB bandwidth, -108 dB THD @ 20 kHz and 22 V/ μ s slew rate are provided with a low supply current of 2.6 mA per amplifier. The AD823 drives up to 500 pF of direct capacitive load as a follower, and provides an output current of 15 mA, 0.5 V from the supply rails. This allows the amplifier to handle a wide range of load conditions.

This combination of ac and dc performance, plus the outstanding load drive capability results in an exceptionally versatile amplifier for applications such as A/D drivers, high-speed active filters, and other low voltage, high dynamic range systems.

REV. 0

Information furnished by Analog Devices is believed to be accurate and reliable. However, no responsibility is assumed by Analog Devices for its use, nor for any infringements of patents or other rights of third parties which may result from its use. No license is granted by implication or otherwise under any patent or patent rights of Analog Devices.

CONNECTION DIAGRAM
8-Pin Plastic Mini-DIP
and
8-Lead SOIC



The AD823 is available over the industrial temperature range of -40 $^{\circ}$ C to +85 $^{\circ}$ C and is offered in both 8-pin plastic DIP and SOIC packages.

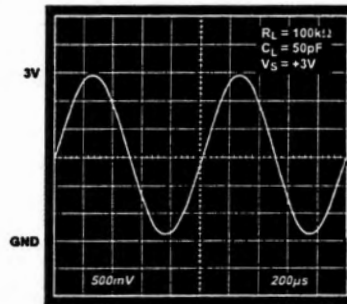


Figure 1. Output Swing, $V_S = +3$ V, $G = +1$

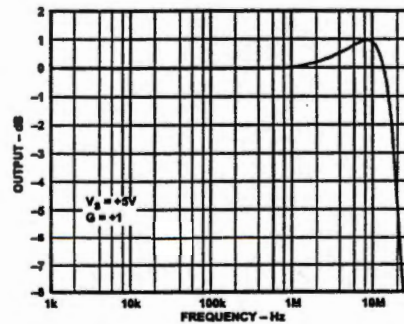


Figure 2. Small Signal Bandwidth, $G = +1$

© Analog Devices, Inc., 1995

One Technology Way, P.O. Box 9106, Norwood, MA 02062-9106, U.S.A.
Tel: 617/329-4700 Fax: 617/326-8703

AD823—SPECIFICATIONS

(@ $T_A = +25^\circ\text{C}$, $V_S = \pm 15\text{ V}$, $R_L = 2\text{ k}\Omega$ to 0 V , unless otherwise noted)

Parameter	Conditions	AD823A			Units
		Min	Typ	Max	
DYNAMIC PERFORMANCE					
-3 dB Bandwidth, $V_O \leq 0.2\text{ V p-p}$	$G = +1$	12	16		MHz
Full Power Response	$V_O = 2\text{ V p-p}$		4		MHz
Slew Rate	$G = -1$, $V_O = 10\text{ V Step}$	17	25		V/ μs
Settling Time	$G = -1$, $V_O = 10\text{ V Step}$		550		ns
to 0.1%			650		ns
to 0.01%					
NOISE/DISTORTION PERFORMANCE					
Input Voltage Noise	$f = 10\text{ kHz}$		16		nV/ $\sqrt{\text{Hz}}$
Input Current Noise	$f = 1\text{ kHz}$		1		fA/ $\sqrt{\text{Hz}}$
Harmonic Distortion	$R_L = 600\ \Omega$, $V_O = 10\text{ V p-p}$, $f = 20\text{ kHz}$		-90		dBc
Crosstalk					
$f = 1\text{ kHz}$	$R_L = 5\text{ k}\Omega$		-130		dB
$f = 1\text{ MHz}$	$R_L = 5\text{ k}\Omega$		-93		dB
DC PERFORMANCE					
Initial Offset			0.7	3.5	mV
Max Offset Over Temperature			1.0	7	mV
Offset Drift			2		$\mu\text{V}/^\circ\text{C}$
Input Bias Current	$V_{CM} = 0\text{ V}$		5	30	pA
	$V_{CM} = -10\text{ V}$		60		pA
at T_{MAX}	$V_{CM} = 0\text{ V}$		0.5	5	nA
Input Offset Current			2	20	pA
at T_{MAX}			0.5		nA
Open-Loop Gain	$V_O = +10\text{ V to } -10\text{ V}$ $R_L = 2\text{ k}\Omega$	30	60		V/mV
T_{MIN} to T_{MAX}		30			V/mV
INPUT CHARACTERISTICS					
Input Common-Mode Voltage Range		-15.2 to 13	-15.2 to 13.8		V
Input Resistance			10^{13}		Ω
Input Capacitance			1.8		pF
Common-Mode Rejection Ratio	$V_{CM} = -15\text{ V to } +13\text{ V}$	66	82		dB
OUTPUT CHARACTERISTICS					
Output Voltage Swing					
$I_L = \pm 100\ \mu\text{A}$			-14.95 to +14.95		V
$I_L = \pm 2\text{ mA}$			-14.92 to +14.92		V
$I_L = \pm 10\text{ mA}$			-14.75 to +14.75		V
Output Current	$V_{OUT} = -14.5\text{ V to } +14.5\text{ V}$		17		mA
Short Circuit Current	Sourcing to 0 V		80		mA
	Sinking to 0 V		60		mA
Capacitive Load Drive	$G = +1$		500		pF
POWER SUPPLY					
Operating Range		+3		+36	V
Quiescent Current	T_{MIN} to T_{MAX} , Total		7.0	8.4	mA
Power Supply Rejection Ratio	$V_S = +5\text{ V to } +15\text{ V}$, T_{MIN} to T_{MAX}	70	80		dB

Specification subject to change without notice.

AD823

ABSOLUTE MAXIMUM RATINGS¹

Supply Voltage	+36 V
Internal Power Dissipation ²	
Plastic Package (N)	1.3 Watts
Small Outline Package (R)	0.9 Watts
Input Voltage (Common Mode)	$\pm V_S$
Differential Input Voltage	± 1.2 V
Output Short Circuit Duration	
.....	Observe Power Derating Curves
Storage Temperature Range N, R	-65°C to +125°C
Operating Temperature Range	-40°C to +85°C
Lead Temperature Range (Soldering 10 sec)	+300°C

NOTES

¹Stresses above those listed under "Absolute Maximum Ratings" may cause permanent damage to the device. This is a stress rating only and functional operation of the device at these or any other conditions above those indicated in the operational section of this specification is not implied. Exposure to absolute maximum rating conditions for extended periods may affect device reliability.

²Specification is for device in free air:

8-Pin Plastic Package: $\theta_{JA} = 90^\circ\text{C/Watt}$

8-Pin SOIC Package: $\theta_{JA} = 160^\circ\text{C/Watt}$

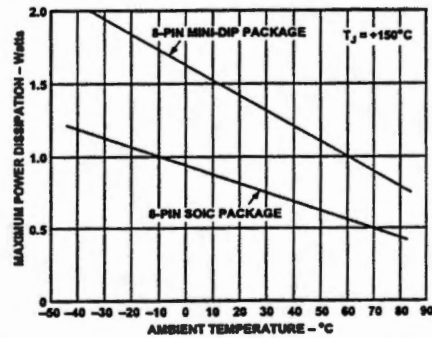


Figure 3. Maximum Power Dissipation vs. Temperature

ORDERING GUIDE

Model	Temperature Range	Package Description	Package Option
AD823AN	-40°C to +85°C	8-Pin Plastic DIP	N-8
AD823AR	-40°C to +85°C	8-Pin Plastic SOIC	SO-8
AD823AR-REEL	-40°C to +85°C	SOIC on Reel	SO-8

CAUTION

ESD (electrostatic discharge) sensitive device. Electrostatic charges as high as 4000 V readily accumulate on the human body and test equipment and can discharge without detection. Although the AD823 features proprietary ESD protection circuitry, permanent damage may occur on devices subjected to high energy electrostatic discharges. Therefore, proper ESD precautions are recommended to avoid performance degradation or loss of functionality.

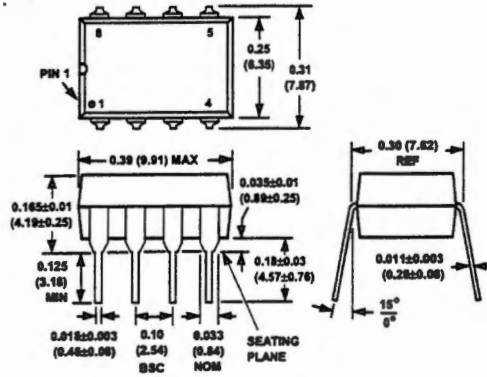


OUTLINE DIMENSIONS

Dimensions shown in inches and (mm).

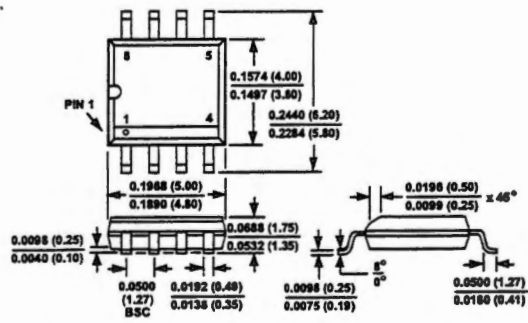
8-Lead Plastic DIP

(N-8)



8-Lead Plastic SOIC

(SO-8)



Appendix C

Micrologger Data Acquisition Program

GILBERT
100% COTTON

```

;{CR23X}
;
*Table 1 Program
  01: .01      Execution Interval (seconds)

1: Beginning of Loop (P87)
  1: 0      Delay
  2: 0      Loop Count

  2: If Flag/Port (P91)
    1: 51      Do if Port 1 is Low
    2: 31      Exit Loop if True

  3: Burst Measurement (P23)
    1: 1      Input Channels per Scan
    2: 15     5000 mV, Fast Range
    3: 2      In Chan
    4: 0      Trig/Trig/Dest/Meas Options
    5: 5      Time per Scan (msec)
    6: 5      Scans (in thousands)
    7: 0      Samples before Trigger
    8: 0      mV Limit
    9: 0      mV Excitation
   10: 1      Loc [ t_1      ]
   11: 1      Mult
   12: 0      Offset

  4: Do (P86)
    1: 10     Set Output Flag High (Flag 0)

  5: Sample (P70)
    1: 5000   Reps
    2: 1      Loc [ t_1      ]

6: End (P95)

```

```

*Table 2 Program
  02: 0.0000  Execution Interval (seconds)

```

```

*Table 3 Subroutines

```

```

End Program

```

```

-Input Locations-
1 t_1      39 1 1
2 t_2      42 0 0
3 t_3      42 0 0
4 t_4      42 0 0
5 t_5      42 0 0
6 t_6      42 0 0
7 t_7      42 0 0
8 t_8      42 0 0
9 t_9      42 0 0

```

10 t_10 42 0 0
11 t_11 42 0 0
12 t_12 42 0 0
13 t_13 42 0 0
14 t_14 42 0 0
15 t_15 42 0 0
16 t_16 42 0 0
17 t_17 42 0 0
18 t_18 42 0 0
19 t_19 42 0 0
20 t_20 42 0 0
21 t_21 42 0 0
22 t_22 42 0 0
23 t_23 42 0 0
24 t_24 42 0 0
25 t_25 42 0 0
26 t_26 42 0 0
27 t_27 42 0 0
28 t_28 42 0 0
5000 t_5000 50 0 0

-Program Security-

0000

0000

0000

-Mode 4-

-Final Storage Area 2-

0

-CR10X ID-

0

-CR10X Power Up-

3

-CR10X Compile Setting-

3

-CR10X RS-232 Setting-

-1

WILLIAMS

100% SOLUTION

Appendix D

MatLab Post-Processing Program

```

clc
clear

filnum=input('What file please ','s');
%step=input('What step size ');
mph=input('What is the speed in MPH ');
step=30;
speed=mph*17.6;

filename=strcat(num2str(filnum),'.txt');

m=dlmread(filename,','); %Reading matrix file file
ddd=26

[r,c]=size(m); %Sizing the matrix
bigmatrix=r*c;

new=zeros(1,r*c); %Making a matrix of zeros 1 row wide many columns
wide

d=1;
for y=1:r %Taking multiple row and column matrix apart and placing
it in a single row
    w=m(y,:);
    new(1,[d:(d+c-1)])=w;
    d=c+d;
end

[r,c]=size(new); %Sizing new matrix

b=1;
dl=1;
opp=69
for g=1:r*c %Taking out every 5001 points

if g~=dl

    reduce(b)=new(g); %Taking reduced data and placing it in a new
matrix

    b=b+1;
    else
    dl=dl+5001;
end
end

deee=15
new1=reduce'; % Placing matrix in a column

[r,c]=size(new1); %Sizing the new matrix

plot(1:r,new1) %Ploting the new matrix

```

figure

```
co=1;
for col=c
    for row=1:5:r-5
        move=newl(row:row+4,col); % Taking the avg of the matrix to
smooth it
        smooth(co)=mean(move);
        co=co+1;
    end
end

filename1=strcat('avg',num2str(filnum),'.txt'); %Writing avg data to
file so easier to play with latter
dlmwrite(filename1,smooth,','); % Takes data from column form and
places it into a row.Must change it back

[r,c]=size(smooth);
plot(1:c,smooth) %Make sure that this matrix is in one row
multiple columns
figure

for v=step+1:r*c-step
    rise=smooth(v+step)-smooth(v-step); % Taking the derivative of the
data in the smoothed matrix
    run=2;
    deriv(v-step)=rise/run;
end

deriv2=deriv';
[r,c]=size(deriv2); %Making new matrix of deriv in a column

co=1;
for col=c
    for row=1:3:r-3
        move=deriv2(row:row+2,col); % Taking the avg of the deriv matrix
to smooth it
        dsmooth(co)=mean(move);
        co=co+1;
    end
end
[r1,c1]=size(dsmooth);
plot(1:c1,dsmooth) % Plotting the avg. derivative
figure

[r,c]=size(deriv);
plot(1:c,deriv) % Plotting the derivative
```

```

sampsiz=800*(1/speed)*2.5*((r1*c1)/bigmatrix); % Samples present per
stalk for counting function
                                % r and c terms come from the
matrix used for the counting loop

count=0;
counter=sampsiz;
counter2=0;      %Setting counters for for stalk recognition loop
for h=1:r1*c1

    if dsmooth(h)>=100
        if counter>=sampsiz      %Loop that sets flag if voltage above 100
milivolts
            counter=1;          % Counters are also started and maintained
here
            counter2=1;         %Loop also insures that stalks aren't
doubled counted
            flag=1;
        end
    end

    if dsmooth(h)<=10      % Enters this loop if voltage less then 10 and
then sees if flag=1

        if flag==1
            count=count+1; % Count is advanced and flag set back to
zero
            flag=0;
        end
    end
    if counter2>=sampsiz+10 %Loop to insure that multiple stalks are
counted if voltage never drops
        if flag==1
            count=count+1; % Counters are advanced here for multiple
counts
            counter2=1;
        end
    end
    counter=counter+1;      %Final stalk count recorded and loop starts
over for next point
    counter2=counter2+1;
end

Stalks=count

```

Vita

Newman Edward Webb II was born in Knoxville, Tennessee on August 17, 1974.

He graduated from Central High School in May of 1993. He received a Bachelor of Science (1998) and a Master of Science in Agricultural Engineering (2001) from The University of Tennessee.

OLBERT
1000000000

8829 6227 30
07-18-01 ✓ MFB 